cmgh
CELLULAR AND MOLECULAR GASTROENTEROLOGY AND HEPATOLOGY

ORIGINAL RESEARCH

FGL2–MCOLN3-Autophagy Axis–Triggered Neutrophil Extracellular Traps Exacerbate Liver Injury in Fulminant Viral Hepatitis

Xitang Li,[1,2,3] Qiang Gao,[1,2,3,*] Wenhui Wu,[1,2,3,*] Suping Hai,[1,2,3,*] Junjian Hu,[1,2,3,*] Jie You,[1,2,3] Da Huang,[1,2,3] Hongwu Wang,[1,2,3,§] Di Wu,[1,2,3] Meifang Han,[1,2,3] Dong Xi,[1,2,3] Weiming Yan,[1,2,3] Tao Chen,[1,2,3] Xiaoping Luo,[4] Qin Ning,[1,2,3,§] and Xiaojing Wang[1,2,3,§]

[1]Department and Institute of Infectious Diseases, Tongji Hospital, Tongji Medical College, Huazhong University of Science and Technology, Wuhan, Hubei, China; [2]National Medical Center for Major Public Health Events, Wuhan, China; [3]State Key Laboratory for Zoonotic Diseases, Tongji Hospital, Tongji Medical College, Huazhong University of Science and Technology, Wuhan, Hubei, China; and [4]Department and Institute of Pediatrics, Tongji Hospital, Tongji Medical College, Huazhong University of Science and Technology, Wuhan, Hubei, China

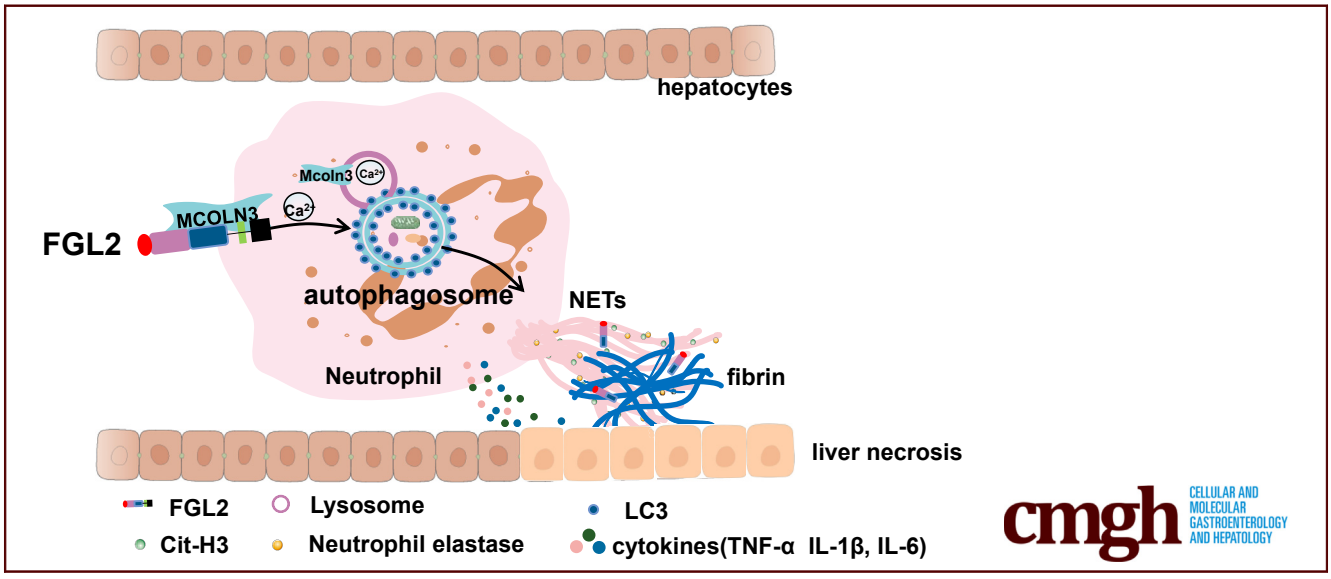

SUMMARY

We clarified that increased neutrophil extracellular traps (NETs) were observed in fulminant viral hepatitis, but not in acetaminophen-treated mice. NETs depletion improved the survival rate in fulminant viral hepatitis by inhibiting fibrin deposition and inflammation. In depth, NETs formation was modulated by the fibrinogen-like protein 2–mucolipin 3–autophagy axis.

BACKGROUND & AIMS: Fulminant viral hepatitis (FVH) is a life-threatening disease, but its pathogenesis is not fully understood. Neutrophil extracellular traps (NETs) were an unrecognized link between inflammation and coagulation, which are 2 main features of FVH. Here, we investigated the role and mechanism of NETs in the pathogenesis of FVH.

METHODS: A mouse model of FVH was established by murine hepatitis virus strain-3 infection. Liver leukocytes of infected or uninfected mice were used for single-cell RNA sequencing and whole-transcriptome sequencing. NETs depletion was achieved using DNase 1. Acetaminophen was used to establish a mouse model of non–virus-caused acute liver failure. Clinically, NETs-related markers in liver, plasma, and peripheral neutrophils were assessed in patients with hepatitis B virus (HBV)-related acute liver injury.

RESULTS: Increased hepatic NETs formation was observed in murine hepatitis virus strain-3–infected mice, but not in acetaminophen-treated mice. NETs depletion improved the liver damage and survival rate in FVH by inhibiting hepatic fibrin deposition and inflammation. An adoptive transfer experiment showed that neutrophil-specific fibrinogen-like protein 2 (FGL2) promoted NETs formation. FGL2 was found to directly interact with mucolipin 3, which regulated calcium influx and initiated autophagy, leading to NETs formation. Clinically, increased plasma NETs level was associated with coagulation dysfunction in patients with HBV acute liver injury. Colocalization of FGL2, NETs, and fibrin in liver was observed in these patients.

CONCLUSIONS: NETs aggravated liver injury in FVH by promoting fibrin deposition and inflammation. NETs formation was regulated by the FGL2–mucolipin 3–autophagy axis. Targeting NETs may provide a new strategy for the treatment of FVH. *(Cell Mol Gastroenterol Hepatol 2022;14:1077–1101; https://doi.org/10.1016/j.jcmgh.2022.07.014)*

Keywords: Neutrophil Extracellular Traps; Fibrinogen-Like Protein 2; Fulminant Viral Hepatitis; Mucolipin 3; Autophagy.

Acute liver failure (ALF) is a critical illness with a high mortality rate and can evolve over days or weeks to a fatal outcome. Causes of ALF include acetaminophen (APAP) hepatotoxicity, virus, acute ischemic injury, and autoimmune hepatitis, among which viral-caused ALF, also called fulminant viral hepatitis (FVH), remains a predominant cause of ALF in developing countries.[1] FVH is characterized by massive hepatocyte necrosis, deteriorated liver function, and hepatic encephalopathy. Because of the rapid disease course, the mortality rate of FVH is up to 80% without liver transplantation.[2] Mice infected with murine hepatitis virus strain-3 (MHV-3) ended up with intrahepatic thrombosis and liver necrosis in 3–5 days, serving as a useful animal model for FVH in human beings.[3,4]

Systemic inflammation and intrahepatic activation of coagulation play a central role in the progression of ALF.[5,6] It has been found that neutrophil extracellular traps (NETs) are a previously unrecognized link between inflammation and thrombosis.[7] NETs are web-like structures released from activated neutrophils composed of DNA filaments coated with histones, myeloperoxidase (MPO), neutrophil elastase (NE), and other antimicrobial proteins.[8] NETs limit pathogen dissemination but cause host cell damage at the same time owing to the high local concentration of antimicrobial proteins.[9] Experimental studies have shown that NETs promoted thrombosis in various diseases, including deep vein thrombosis, sepsis, and a variety of liver diseases.[10–12] A very recent clinical study showed that increased markers of NETs were associated with poor outcome of patients with ALF.[13] However, the role and mechanism of NETs in FVH remain unclear.

Fibrinogen-like protein 2 (FGL2) is a novel immune coagulant comprising membrane and soluble forms. Membrane FGL2 can directly cleave prothrombin to thrombin without involvement of factor VII or X,[14] while soluble FGL2 influences dendritic cell maturation and T-cell proliferation.[15] FGL2 is involved not only in microthrombosis,[16–18] but also plays an essential role in inflammatory diseases including viral hepatitis, sepsis, and nonalcoholic steatohepatitis.[14,19,20] Our group and Dr. Gary A. Levy, found that increased FGL2 expression was associated with intravascular fibrin deposition and hepatocyte necrosis in FVH,[14] although the underlying mechanism is not fully understood. Recently, we newly found that membrane FGL2 also was expressed on neutrophils in addition to endothelial cells, macrophages, and regulatory T cells. Considering the modulatory effects of FGL2 on previously reported immune cells,[21] we hypothesized it might as well regulate neutrophil function, especially NETs formation.

In this study, we showed that virus-induced NETs initiated coagulation and a proinflammatory response, contributing to immune-mediated liver injury in FVH. Furthermore, we illustrated that NETs formation was regulated by the FGL2–mucolipin 3 (MCOLN3)–autophagy axis.

Results

Neutrophils Were Increased Significantly in Mice Livers After MHV-3 Infection With Enhanced NETs Formation

Immune response plays a pivotal role in the pathogenesis of liver failure,[22] but little is known about the whole immune microenvironment of infected livers. Here, to characterize the alterations of hepatic leukocytes at single-cell resolution, we used the 10× Chromium platform to sequence mouse liver leukocytes at 60 hours after MHV-3 infection or without infection. We obtained 25,984 transcriptomes (13,202 control; 12,782 MHV-3). Cells were divided into 8 major clusters and the cell composition changes are shown in a bar graph (Figure 1*A*). In innate immunity, we found that the neutrophil number increased significantly, while the amount of monocytes/macrophages, plasma dendritic cells, and basophils decreased in the livers with FVH compared with those in uninfected livers. Natural killer (NK) cells and NK T cells showed no significant change. In adaptive immunity, the number of T cells increased while the number of B cells decreased in MHV-3–infected mice compared with uninfected mice. Innate immunity plays a pivotal role in identifying and removing infected cells as well as modulating adaptive immune response in acute viral infections.[23] Here, we focused on neutrophils, which showed the most remarkable increase in innate immunity. The marker genes (*S100a8*, *S100a9*, *Ly6g*, *Cxcr2*, *Lcn2*, and *Mmp8*) were used to identify neutrophils (Figure 1*B*). Meanwhile, we also performed the whole-transcriptome sequencing to study the activated pathways

*Authors share co-senior authorship; §Authors share co-corresponding authorship

Abbreviations used in this paper: ALF, acute liver failure; ALI, acute liver injury; ALT, alanine aminotransferase; APAP, acetaminophen; AST, aspartate aminotransferase; BM, bone marrow–derived; CHB, chronic hepatitis B; Cit-H3, citrullinated histone-3; ELISA, enzyme-linked immunosorbent assay; FGL2, fibrinogen-like protein 2; FVH, fulminant viral hepatitis; HBV, hepatitis B virus; HC, healthy control; ICAM-1, intercellular adhesion molecule 1; IL, interleukin; INR, international normalized ratio; LC3II, microtubule-associated proteins light chain 3 II; MCOLN3, mucolipin 3; MHV-3, murine hepatitis virus strain-3; ML-SA1, mucolipin synthetic agonist 1; MPO, myeloperoxidase; mRNA, messenger RNA; NE, neutrophil elastase; NETs, neutrophil extracellular traps; NK, natural killer; PAD4, peptidyl arginine deiminase type IV; PBS, phosphate-buffered saline; RNA-seq, RNA sequencing; TAT, thrombin–antithrombin complex; TNF-α, tumor necrosis factor α; WT, wild-type; 3-MA, 3-methyladenine.

Most current article

2352-345X
https://doi.org/10.1016/j.jcmgh.2022.07.014

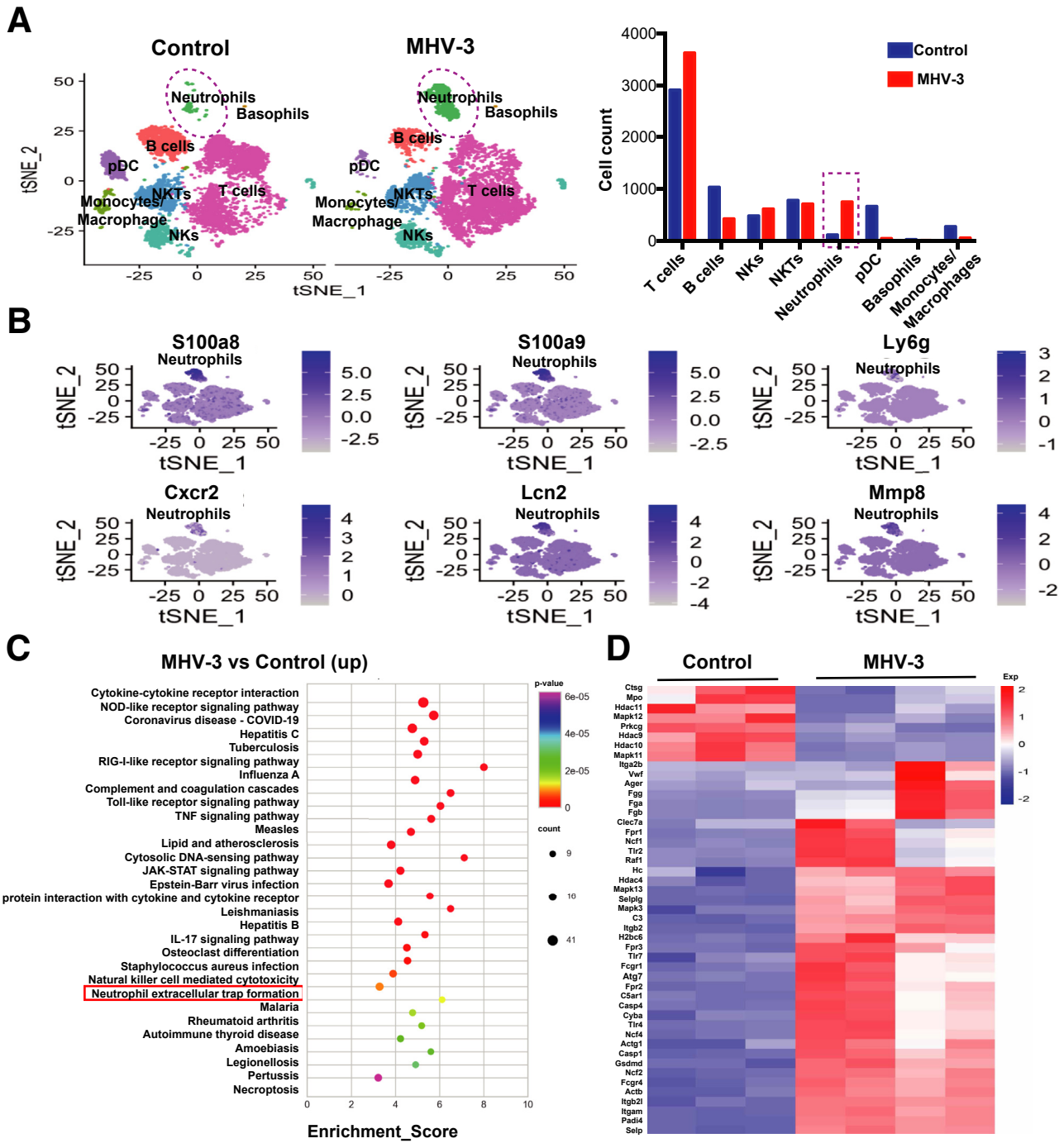

Figure 1. Neutrophils were increased significantly after MHV-3 infection with enhanced NETs formation. Hepatic immune cells of MHV-3–infected mice or control mice were isolated and analyzed using (*A* and *B*) single-cell RNA-seq and (*C* and *D*) whole-transcriptome sequencing. (*A*) Cells were clustered into 8 subpopulations and visualized by t-distributed Stochastic Neighbor Embedding (t-SNE). The changes in cell composition are shown in the bar chart. (*B*) t-SNE maps of hepatic single-cell data within cells are colored based on the expression of neutrophil marker genes (*S100a8*, *S100a9*, *Ly6g*, *Cxcr2*, *Lcn2*, and *Mmp8*). (*C*) The top 500 up-regulated differential genes based on fold change in MHV-3–infected mice compared with controls were used for Kyoto Encyclopedia of Genes and Genomes (KEGG) pathway enrichment (https://www.kegg.jp). The top 30 enrichment pathways based on *P* values are shown in the picture. (*D*) The genes related to the NET formation pathway, which is a defined pathway in KEGG pathways, were selected and displayed in heatmaps in MHV-3–infected mice and controls. The color scale (from blue to red) indicates the gene expression levels. COVID-19, coronavirus disease-2019; Cxcr2, C-X-C Motif Chemokine Receptor 2; JAK, Janus Kinase; Mmp, matrix metallopeptidase; NKT, Natural killer T; NOD, nucleotide-binding oligomerization domain ; pDC, plasmacytoid dendritic cells; RIG, Retinoic acid-inducible gene ; STAT, signal transducer and activator of transcription.

in immune cells after MHV-3 infection. The Kyoto Encyclopedia of Genes and Genomes pathway enrichment of the top 500 up-regulated genes based on fold change showed that the pathway of NETs formation, which was closely related to neutrophil function, was enhanced significantly after virus challenge (Figure 1*C*). In MHV-3–infected mice, there were

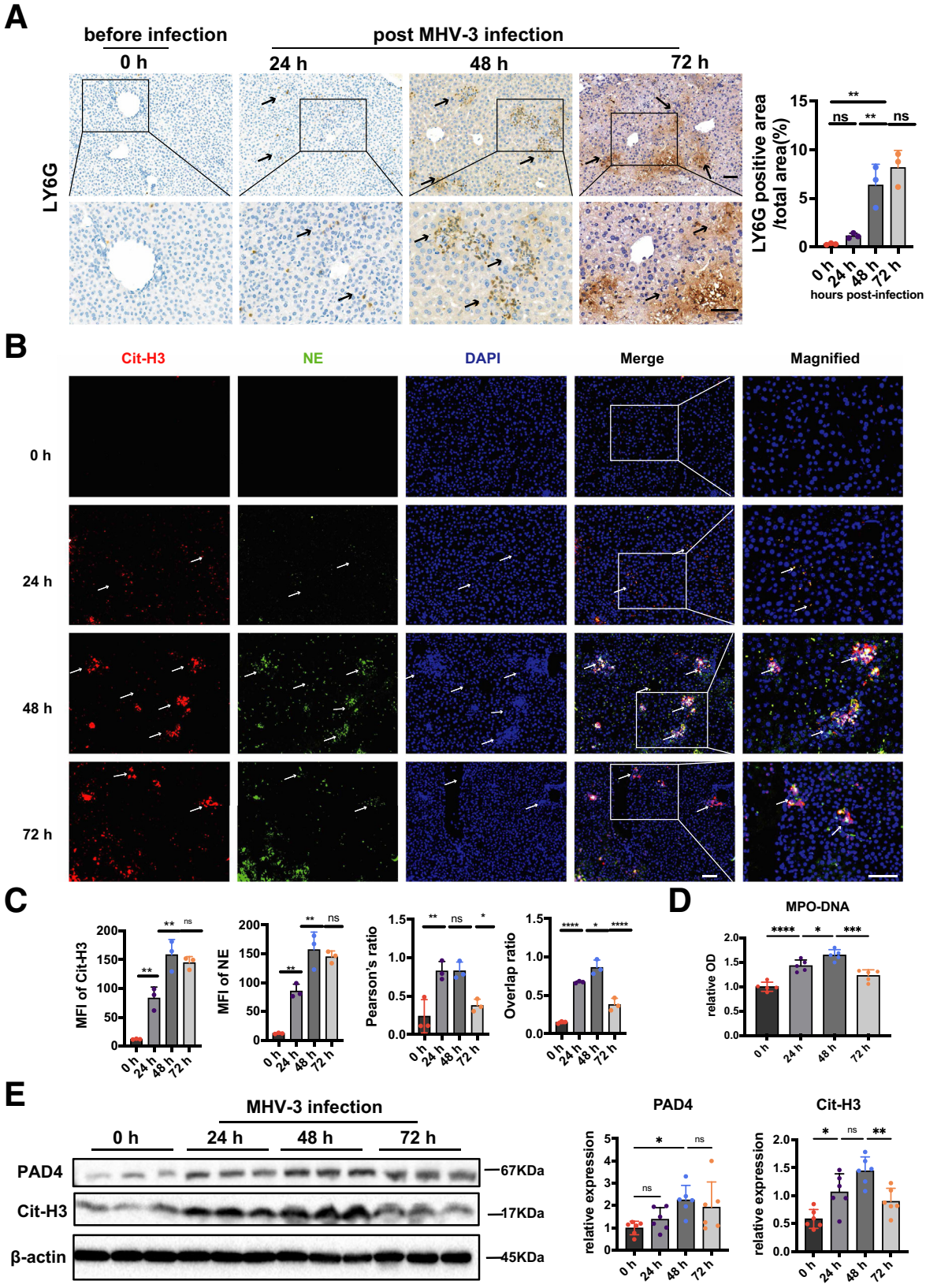

39 up-regulated genes associated with NETs, including *Padi4* and *Mapk3/13*, and so forth, while only 8 genes were down-regulated (Figure 1*D*). These data suggest that MHV-3 infection might trigger neutrophil recruitment and NETs formation in mice livers.

NETs Promoted Hepatic Fibrin Deposition and inflammatory Response, Aggravating Liver Damage in MHV-3–Infected Mice

Previous studies have shown that intrahepatic activation of coagulation and profound inflammatory response contributed to acute liver injury.[5,6,14] Recent studies suggested that NETs served as an unrecognized link between inflammation and coagulation.[7] However, the role and mechanism of NETs in ALF remain unclear. Here, we observed abundant hepatic neutrophil infiltration (Figure 2*A*) and NETs formation as evidenced by increased colocalization of citrullinated histone-3 (Cit-H3) and NE (Figure 2*B* and *C*) in MHV-3–infected mice. This was consistent with our finding from single-cell RNA sequencing (RNA-seq) and whole-transcriptome sequencing (Figure 1), and also was supported by increased serum MPO–DNA level, a recognized biomarker of NETs in circulation[24] (Figure 2*D*). Moreover, increased levels of Cit-H3 and peptidyl arginine deiminase type IV (PAD4), a critical enzyme for NETs generation,[25] also were observed after MHV-3 infection (Figure 2*E*). These data indicate that abundant NETs formation might play an important role in virus-induced ALF.

To identify whether hepatic NETs generation is a universal mechanism in ALF, we also examined NETs markers in an ALF mouse model induced by APAP. Here, APAP treatment caused severe liver necrosis in the centrilobular areas (Figure 3*A*) and increased alanine aminotransferase (ALT) and aspartate aminotransferase (AST) levels (Figure 3*B*). However, although the number of hepatic neutrophils increased (Figure 3*C*), we rarely observed NETs formation in APAP-treated mice livers (Figure 3*D*). Meanwhile, both in vivo (Figure 3*E*) and in vitro (Figure 3*G*) experiments showed that the levels of NETs markers, Cit-H3 and PAD4, decreased after APAP treatment. There was also no significant increase in the levels of serum MPO-DNA (Figure 3*F*). These results suggest that APAP-caused liver damage might be independent of NETs formation, and NETs may play a more important role in viral-induced liver injury.

It was reported that, after virus challenge, NETs not only can trap viruses, but also initiate fibrin deposition and thrombosis, causing tissue damage if too much NETs are released.[7,26] However, little is known about the role of NETs in regulating hepatic microvascular immune-thrombosis in the progression of viral hepatitis. In MHV-3–infected liver, we detected robust fibrin deposition in NETs areas (Figure 4*A*), implying that there might be an association between NETs and thrombosis. To determine the overall effect of NETs in FVH, NETs were depleted after MHV-3 infection (Figure 4*B*). Strikingly, NETs depletion (Figure 4*C*) significantly increased the survival rate from 4% to 29% (Figure 4*D*), with remarkably alleviated pathologic liver injury (Figure 4*E*). Consistent with decreased levels of ALT and AST (Figure 4*F*), we also observed reduced proinflammatory cytokines tumor necrosis factor-α (TNF-α), interleukin (IL)1β, and IL-6 after DNase 1 treatment (Figure 4*G*). In addition, decreased hepatic fibrin deposition (Figure 4*H*) and plasma thrombin–antithrombin complex (TAT) (Figure 4*I*) also were observed after DNase 1 treatment, suggesting that NETs may promote the activation of local and system coagulation, as well as an inflammatory response in FVH.

Considering the exhaustion of neutrophils might be more effective in alleviating liver damage because it could entirely abrogate NETs formation, we also performed neutrophil depletion (Figure 5*A*). Anti-LY6G (1A8) treatment nearly abrogated hepatic neutrophils (Figure 5*B*) and NETs formation (Figure 5*D*). Unexpectedly, no significant difference was found in either survival rate (Figure 5*C*) or liver function (Figure 5*E*), although we observed improved liver histology (Figure 5*F*). These results might be owing to the paradoxic effects of neutrophils. Existing data have shown that neutrophils contribute to antiviral mechanisms by interacting with NK cells and CD8+ T cells,[27] which might counteract the proinflammatory effect of neutrophils. Therefore, the overall effect of neutrophil depletion was quite limited. Taken together, these data indicate that NETs-initiated fibrin deposition and inflammatory response aggravated liver damage in FVH, whereas neutrophils played a paradoxic role in the process.

FGL2 Enhanced NETs Formation and Exacerbated MHV-3–Induced Liver Injury in Mice

Fibrin deposition and microvascular thrombosis play a pivotal role in FVH, in which FGL2 acts as a key regulator for fibrin deposition.[14] Here, we observed up-regulated membrane FGL2 expression on neutrophils after MHV-3 infection (Figure 6*A* and *B*), thus we speculated that FGL2 might be involved in NETs-induced fibrin deposition. Interestingly, the whole-transcriptome sequencing showed that FGL2 deficiency significantly down-regulated NETs formation pathway (Figure 6*C*). Meanwhile, we observed decreased

Figure 2. (***See previous page***). **NETs were excessively released after MHV-3 infection.** (*A*) Neutrophil infiltration in liver was detected by immunochemistry staining with LY6G. *Arrows* indicate neutrophil infiltration. (*B*) Liver samples were detected for NETs by immunofluorescence staining with Cit-H3 (red), neutrophil elastase (green), and 4′,6-diamidino-2-phenylindole (DAPI) (blue). *Arrows* indicate NETs areas. (*C*) The mean fluorescence intensity of Cit-H3, NE, and their colocalization were quantified using ImageJ (National Institutes of Health, Bethesda, MD) analysis software. *Scale bar*: 50 μm. Ten microscopic fields per liver section from 3 mice in each group were counted. (*D*) Serum MPO-DNA levels were detected at indicated time points after MHV-3 infection. n = 5 in each group. (*E*) The expression of hepatic Cit-H3 and PAD4 were measured by Western blot and analyzed by Image lab (Bio-Rad, Hercules, CA). *$P < .05$, **$P < .01$, ***$P < .001$, and ****$P < .0001$, determined by 1-way analysis of variance followed by the Tukey follow-up test.

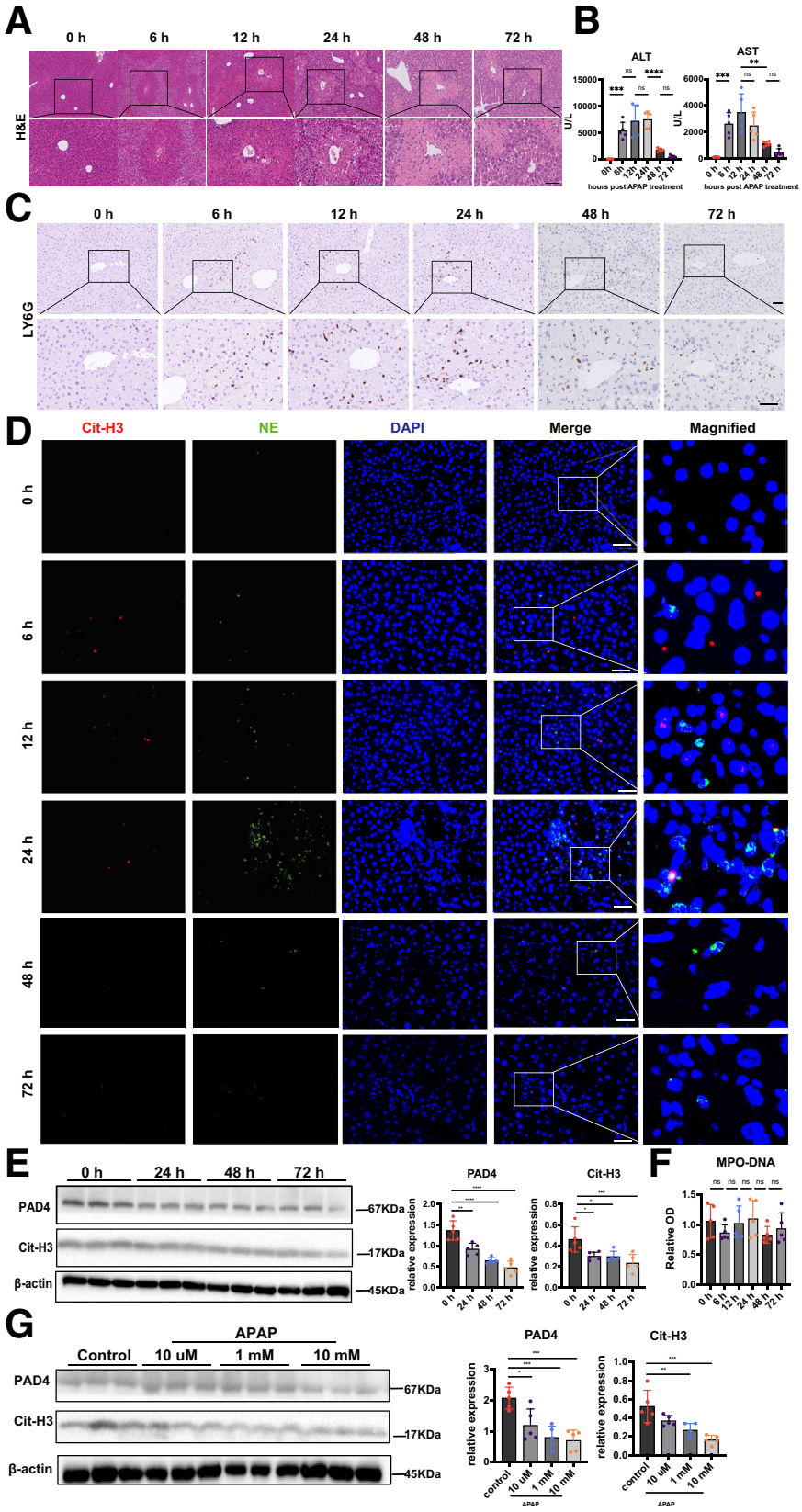

Figure 3. NETs were not induced in APAP-caused liver injury. (*A*) H&E staining of liver tissues at different time points after APAP treatment. (*B*) Serum ALT and AST levels in APAP-treated mice at indicated time points after APAP stimulation. (*C*) Neutrophil infiltration in the livers at different time points after APAP treatment was detected by immunochemistry using anti-LY6G antibody. (*D*) Liver tissues were subjected to immunofluorescence staining with Cit-H3 (red), NE (green), and 4′,6-diamidino-2-phenylindole (DAPI; blue) to detect NETs formation. (*E*) Protein levels of hepatic Cit-H3 and PAD4 were measured by Western blot and analyzed by Image lab. (*F*) Serum MPO-DNA levels were detected at different time points after APAP treatment (n = 5 in each group). (*G*) Neutrophils from the bone marrow of WT mice were challenged with different doses of APAP, and the expression of Cit-H3 as well as PAD4 were detected by Western blot. $^{*}P < .05$, $^{**}P < .01$, $^{***}P < .001$, and $^{****}P < .0001$, determined by 1-way analysis of variance followed by the Tukey follow-up test.

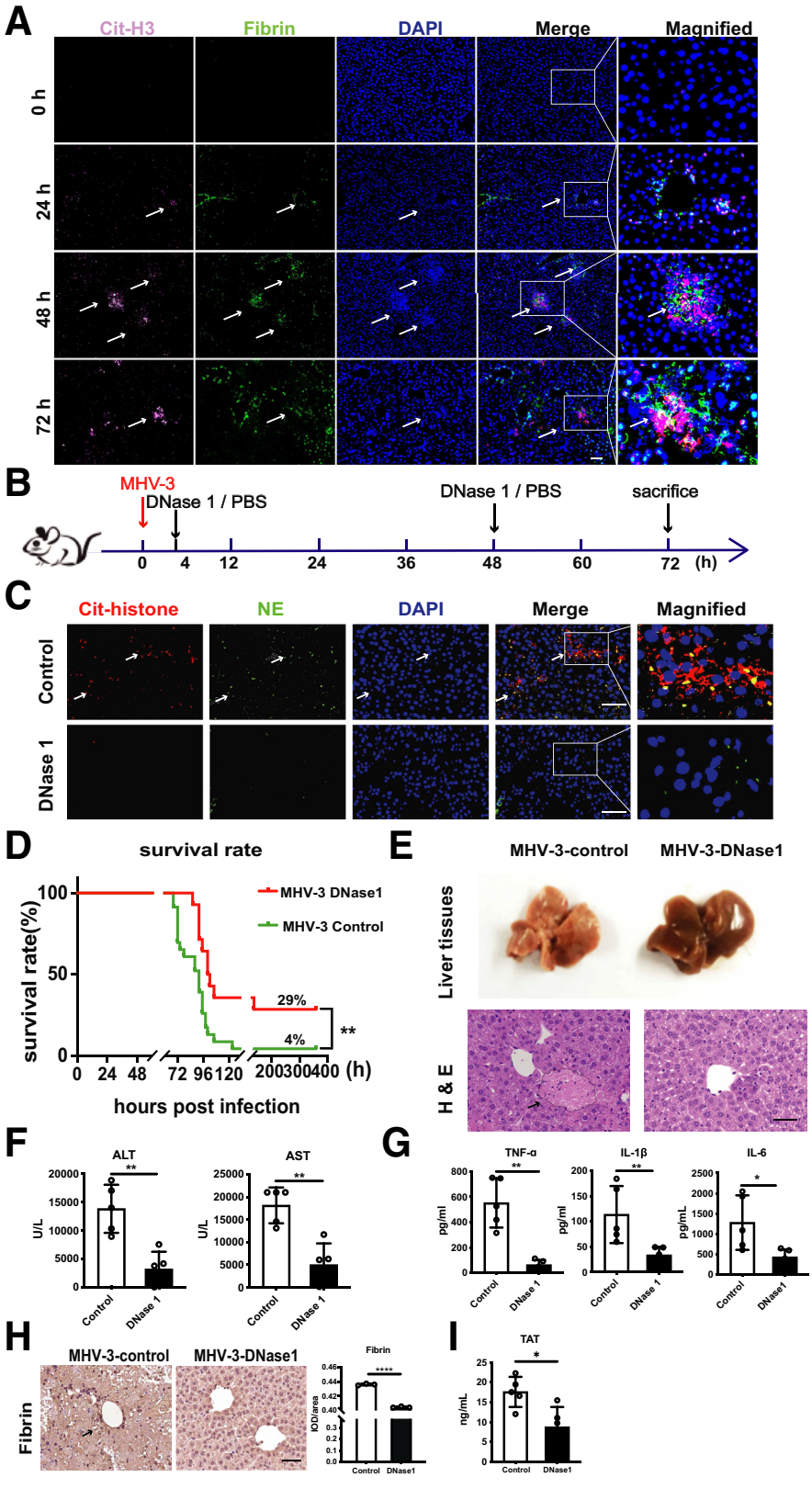

Figure 4. Neutrophil accumulation concomitant with NETs release was related to liver damage induced by MHV-3 infection. (*A*) Colocalization of NETs and fibrin was detected at the indicated time points using immunofluorescent staining with Cit-H3 (pink), fibrin (green), and 4′,6-diamidino-2-phenylindole (DAPI) (blue). (*B*) DNase1 (750 U) (n = 14) or PBS (n = 23) was injected at 4 hours and 48 hours after MHV-3 infection as the time shaft indicated. (*C*) The depletion efficiency was verified by immunofluorescent staining (Cit-H3, red; NE, green) at 72 hours after MHV-3 infection. (*D*) The overall survival rate of mice was monitored. For mice treated with DNase1 or PBS, representative images of (*E*) liver tissues and H&E staining of liver samples are shown at 72 hours after MHV-3 infection. Serum levels of (*F*) ALT, AST, (*G*) TNF-α, IL1β, and IL6 were measured at 72 hours after infection (n = 5 in each group). (*H*) Hepatic fibrin deposition and (*I*) plasma TAT levels were detected in these 2 groups. *Scale bars*: 50 μm. ImageJ analysis software was used for immunochemical and immunofluorescent analysis, 10 microscopic fields per liver section from 3 mice in each group were counted. *$P < .05$, **$P < .01$, and ****$P < .0001$.

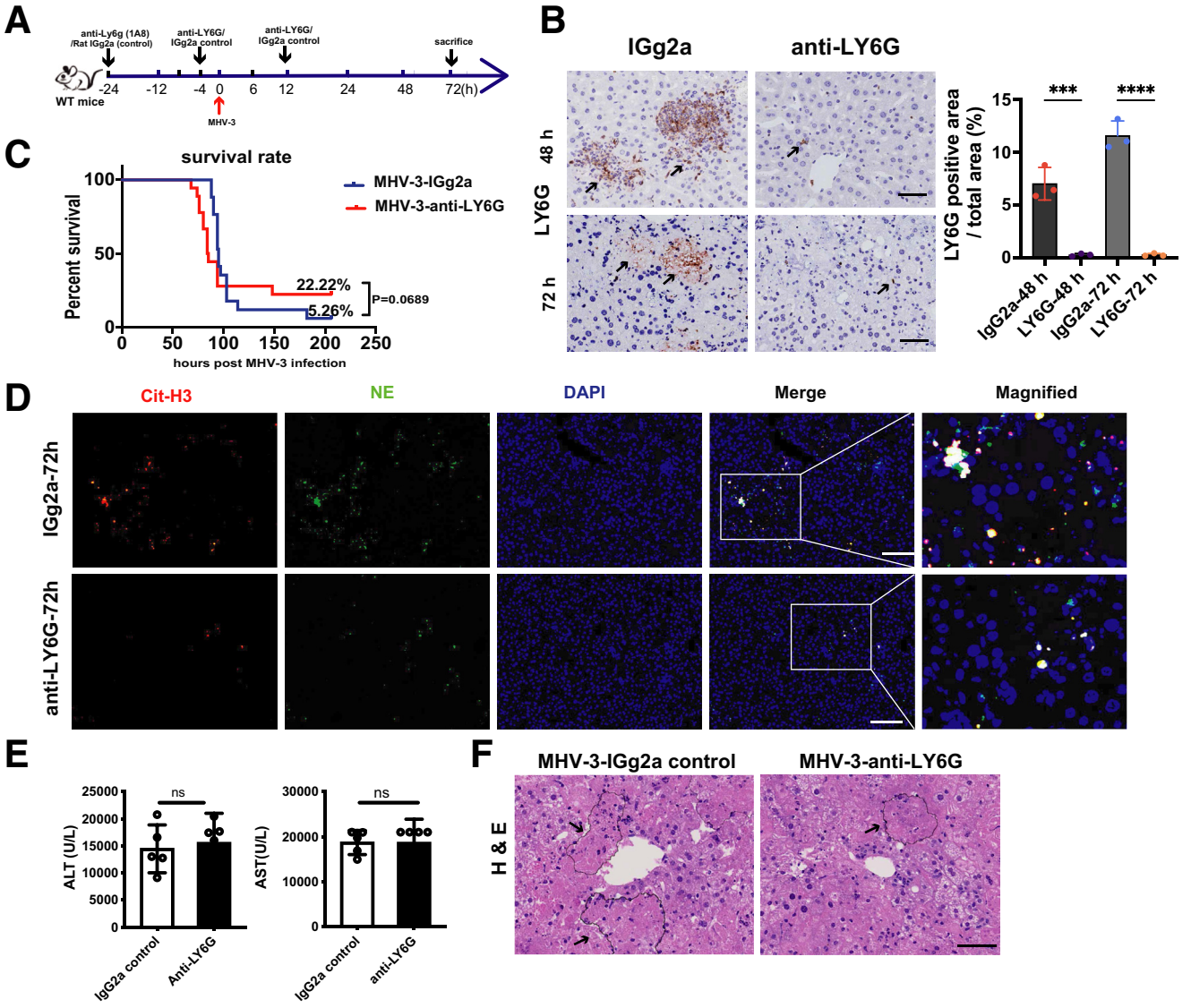

Figure 5. Neutrophil depletion showed no significant protective effect on FVH progression. (*A*) Anti-LY6G was injected intraperitoneally at 24 and 4 hours before, and 12 hours after MHV-3 infection to deplete neutrophils as the time shaft indicated. Rat IGg2a was used as a control. (*B*) The depletion efficacy of neutrophils at 48 and 72 hours after infection was verified by immunochemical staining of LY6G. *Arrows* indicate representative areas of neutrophils. *Scale bars*: 50 μm. (*C*) The overall survival rate of mice was observed (n = 15–18 in each group). Survival rate was compared by using the log-rank test. (*D*) Hepatic NETs formation after neutrophil depletion was detected by immunofluorescent staining (Cit-H3, red; NE, green). (*E*) Liver enzymes (ALT, AST) and (*F*) liver histology was examined at 72 hours after MHV-3 infection. For bar graphs, n = 5 in each group. Statistical analysis was performed by unpaired Student *t* test. ***$P < .001$, ****$P < .0001$. DAPI, 4′,6-diamidino-2-phenylindole.

hepatic colocalization of Cit-H3 and NE (Figure 6*D*), as well as reduced serum MPO-DNA level (Figure 6*E*) in *fgl2*$^{-/-}$ mice compared with wild-type (WT) controls, indicating less NETs release upon FGL2 deficiency. In vitro, we stimulated bone marrow–derived (BM) neutrophils with MHV-3, and *fgl2*$^{-/-}$ BM neutrophils showed decreased capacity of NETs release as evidenced by reduced Sytox Green (Invitrogen, Carlsbad, CA) staining (Figure 6*F*). In MHV-3–infected mice, FGL2 deficiency decreased plasma TAT levels (Figure 6*G*), as well as hepatic NETs formation and fibrin deposition (Figure 6*H*). Consistently, we observed alleviated histopathologic lesions (Figure 7*A*), improved liver appearances (Figure 7*B*) and liver function (ALT and AST) (Figure 7*C*), as well as decreased proinflammatory cytokines (TNF-α, IL1β, and IL6) (Figure 7*D*) in *fgl2*$^{-/-}$ mice.

To further verify the role of FGL2 in NETs formation, 4 × 10^6 WT and *fgl2*$^{-/-}$ BM neutrophils were adoptively transferred into *fgl2*$^{-/-}$ mice (Figure 7*E* and *F*). The adoptive transfer of WT BM neutrophils led to exacerbation of disease progression, which was evidenced by aggravated histologic lesions (Figure 7*G*), increased levels of ALT and AST (Figure 7*H*), along with increased proinflammatory cytokines (TNF-α, IL1β, and IL6) (Figure 7*I*) compared with that of *fgl2*$^{-/-}$ BM neutrophils and controls. Notably, enhanced NETs formation (Figure 7*J* and *K*) and augmented fibrin deposition (Figure 7*L*) also were detected in livers of mice

injected with WT BM neutrophils, but not in those injected with *fgl2*$^{-/-}$ BM neutrophils or controls. These results indicated that neutrophil-specific FGL2 induced NETs formation and subsequent fibrin deposition and inflammatory response, causing tissue damage in FVH.

It is worth mentioning that the neutrophil number was as well reduced upon fgl2 deficiency (Figure 8*A* and *B*), suggesting that a decrease of the hepatic NETs level might be owing in part to altered neutrophil numbers in MHV-3 infection. To identify the factors influencing neutrophil

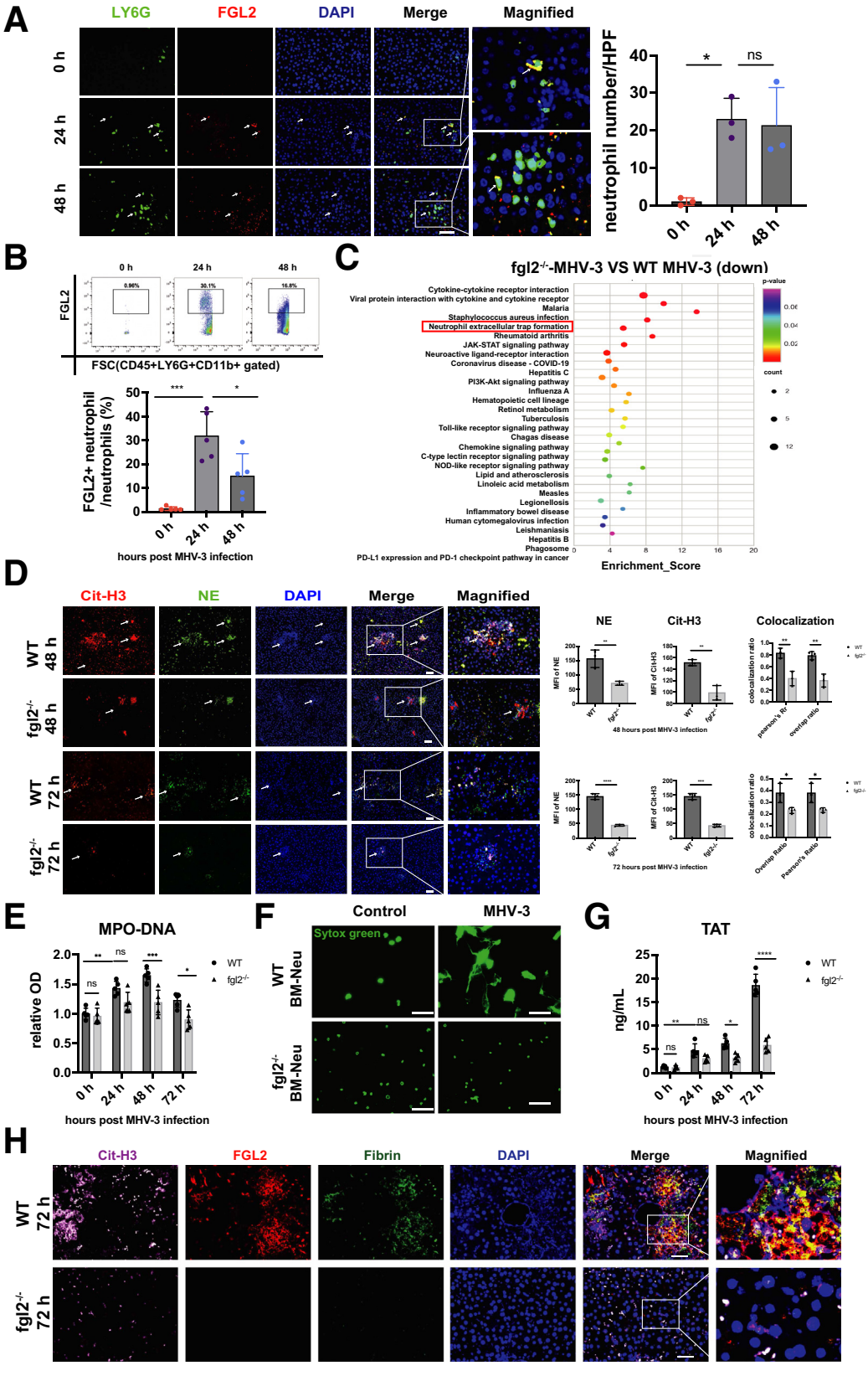

accumulation, we detected intercellular adhesion molecule-1 (ICAM-1), E-selectin, and L-selectin, which are key mediators in modulating neutrophil transendothelial infiltration.[28] Compared with WT mice, *fgl2*$^{-/-}$ mice showed a lower level of hepatic ICAM-1, while E-selectin and L-selectin remained unchanged (Figure 8*C*). In addition, we observed decreased messenger RNA (mRNA) levels of intrahepatic *Cxcl1*, *Cxcl2*, and *Cxcr2* upon fgl2 deficiency (Figure 8*D*), suggesting that FGL2 affected neutrophil recruitment to the liver. However, the underlying mechanism needs to be elucidated further. Collectively, these data suggest that FGL2 deficiency not only reduced the capacity of neutrophils to generate NETs, but also changed the neutrophil chemotactic microenvironment.

NETs Formation Was Induced in FVH Through the FGL2–MCOLN3–Autophagy Axis

To investigate the mechanism of how FGL2 triggered NETs formation, we screened the most recognized pathways of NETs formation, including AKT, p38–mitogen-activated protein kinase, extracellular regulated protein kinase, and mitogen-activated protein kinase.[29] However, it seemed that neutrophil FGL2 had no obvious impact on these pathways in FVH (Figure 9*A* and *B*). Previous studies have shown that autophagy is required for neutrophil-induced inflammation and could mediate NETs formation under various stimulations.[30,31] Therefore, we next explored the potential role of FGL2 in autophagy induction. Concomitant with decreased expression of Cit-H3 and PAD4, the critical markers of NETs formation, we observed down-regulated hepatic autophagy, manifested as reduced microtubule-associated proteins light chain 3 II (LC3II) and Beclin 1 levels and increased sequestosome 1 (P62/Sqstm1) level in *fgl2*$^{-/-}$ mice compared with WT mice (Figure 10*A*). In vitro, we stimulated neutrophils with MHV-3, which showed a similar result (Figure 10*B*). Immunofluorescence showed reduced LC3 puncta cells in *fgl2*$^{-/-}$ BM neutrophils compared with WT BM neutrophils after MHV-3 infection and this could be blunted by 3-methyladenine (3-MA) treatment (Figure 10*C*). Transmission electron microscopy also showed a significant decrease of double-membrane structures, which are typical features of autophagosome,[32] in *fgl2*$^{-/-}$ BM neutrophils compared with WT BM neutrophils after MHV-3 stimulation (Figure 10*D*). Moreover, inhibition of autophagy using 3-MA blocked FGL2-mediated NETs formation in vitro (Figure 10*E* and *F*), indicating that FGL2-induced autophagy is essential to NETs release.

To elucidate the molecular mechanisms through which FGL2 modulates autophagy, we searched for potential FGL2-interacting proteins in the search tool for the retrieval of interacting genes/proteins (STRING) database, where we found that FGL2 has a potential functional connection with MCOLN3 (Figure 11*A*), an inward rectifying Ca^{2+} channel that plays a key role in regulating autophagy.[33] The prediction score for the FGL2–MCOLN3 interaction was 0.778, which ranked second among the functional FGL2-centric protein-interaction networks (Figure 11*B*). We then isolated primary hepatic neutrophils and performed co-immunoprecipitation assays, which suggested a marked interaction between FGL2 and MCOLN3 (Figure 11*C*). Furthermore, FGL2 was found to colocalize with MCOLN3 by immunofluorescent staining in BM neutrophils after MHV-3 stimulation (Figure 11*D*). A number of studies have shown that MCOLN3 is recruited and provides Ca^{2+} for the fusion process in autophagosome biogenesis upon autophagy induction,[33,34] we thus wondered whether FGL2 could influence the activation of MCOLN3 to release Ca^{2+}. A significant increase of Ca^{2+} influx was detected only in WT BM neutrophils after MHV-3 stimulation, but not in *fgl2*$^{-/-}$ BM neutrophils, and this effect could be reversed by using anti-MCOLN3 antibody or MCOLN3 agonist, mucolipin synthetic agonist 1 (ML-SA1) (Figure 11*E*). We also found that anti-MCOLN3 antibody inhibited autophagy in WT BM neutrophils, while ML-SA1 treatment enhanced autophagy in *fgl2*$^{-/-}$ BM neutrophils after MHV-3 infection (Figure 11*F*). Interestingly, the alterations of NETs formation in MHV-3–infected WT and *fgl2*$^{-/-}$ BM neutrophils could be reversed by anti-MCOLN3 antibody or MCOLN3 agonist (ML-SA1) (Figure 11*G*). These data show that FGL2 interacted with MCOLN3, leading to induction of Ca^{2+} influx and activation of autophagy, which ultimately boosted NETs release.

NETs Formation Was Correlated With Dysregulated Coagulation and Fibrin Deposition in Patients With Hepatitis B Virus Acute Liver Injury

Acute hepatitis B virus (HBV) infection and acute exacerbations of chronic HBV infection are the most frequent causes of human FVH.[35] Given the essential role of NETs in

Figure 6. (***See previous page***). **FGL2 deficiency repressed NETs formation and subsequent fibrin deposition after MHV-3 infection.** FGL2 expression on hepatic neutrophils was observed at the indicated time points using (*A*) immunofluorescent staining (neutrophils, green; FGL2, red; nucleus, blue) and (*B*) flow cytometry (n = 5 in each group). (*C*) Isolated hepatic leukocytes were subjected to whole-transcriptome sequencing. The top 100 down-regulated genes based on fold change in *fgl2*$^{-/-}$ mice compared with WT mice after MHV-3 infection were used for Kyoto Encyclopedia of Genes and Genomes (KEGG) enrichment (https://www.kegg.jp). The top 30 enriched KEGG pathways based on *P* values are shown in the picture. (*D*) NETs formation was detected by immunofluorescent staining of Cit-H3 and NE at 48 and 72 hours after MHV-3 infection. (*E*) Serum MPO-DNA levels were measured at different time points after MHV-3 infection. (*F*) WT or *fgl2*$^{-/-}$ BM neutrophils were stimulated with MHV-3 in vitro. The NETs formation was detected 3 hours after infection by fluorescent staining with Sytox Green. (*G*) The levels of plasma TAT were detected at different time points in WT and *fgl2*$^{-/-}$ mice. n = 5 in each group. (*H*) Representative immunofluorescence staining of Cit-H3 (pink), FGL2 (red), and fibrin (green) staining in liver sections at 72 hours after infection. *Scale bars*: 50 μm. For immunofluorescent analysis, 10 microscopic fields per liver section from 3 mice in each group were counted using ImageJ. **P* < .05, ***P* < .01, ****P* < .001, and *****P* < .0001, determined by 1-way analysis of variance. COVID-19, coronavirus disease-2019; DAPI, 4′,6-diamidino-2-phenylindole; HPF, high-power field; NOD, nucleotide-binding oligomerization domain; OD, optical density; PD-1, programmed death-1; PD-L1, programmed death-ligand 1.

exacerbating liver damage in murine FVH, we speculated that NETs also might be involved in the development and progression of HBV acute liver injury (ALI)/ALF. In this study, we enrolled 28 patients with HBV ALI/ALF, 45 patients with chronic hepatitis B (CHB), and 45 healthy controls (HCs). The characteristics of these patients are

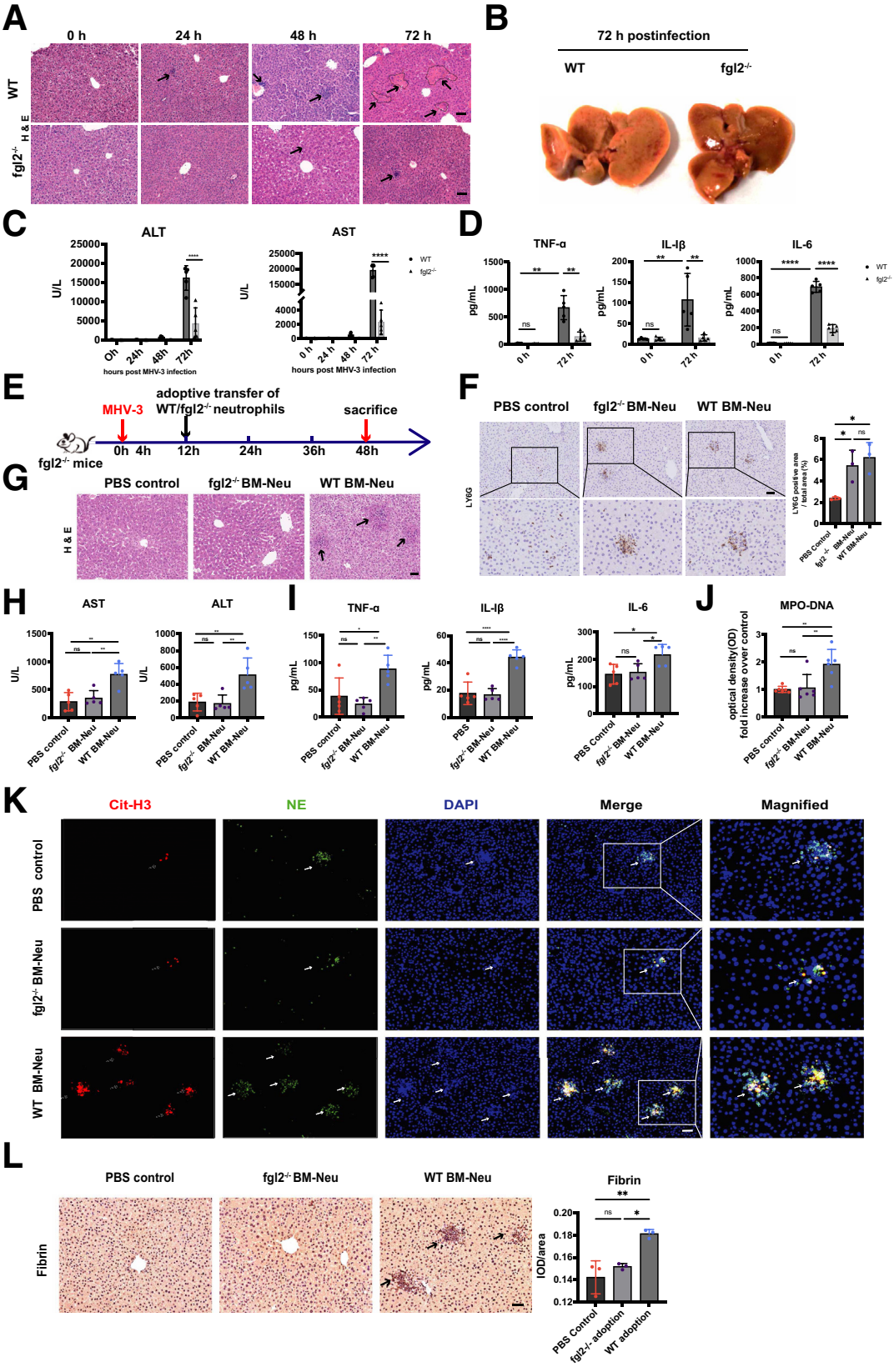

presented in Table 1. We observed significantly increased plasma MPO and MPO-DNA levels in patients with HBV ALI/ALF compared with controls (CHB and HC) (Figure 12*A*). Meanwhile, plasma MPO levels were correlated with prothrombin time activity and international normalized ratio (INR) (Figure 12*B*), and MPO-DNA levels were associated positively with plasma TAT expression (Figure 12*C*), implying that NETs might be associated with dysregulated coagulation and contribute to the disease progression of HBV ALI/ALF. Next, we attempted to clarify whether FGL2 facilitated NETs release in patients was similar to what we found in animal models. Because of the limitation of acquiring primary hepatic neutrophils, we isolated peripheral neutrophils and observed a significantly up-regulated mRNA expression of *FGL2* (Figure 12*D*) in neutrophils of patients with HBV ALI/ALF compared with controls. Furthermore, we observed that FGL2+ neutrophils released a much higher amount of NETs than FGL2- neutrophils did in patients with HBV ALI/ALF (Figure 12*E*). In liver, inflammatory cell infiltration was increased dramatically (Figure 12*F*), accompanied by up-regulated NETs formation (Figure 12*G*) in patients with HBV ALF. Moreover, increased colocalization of FGL2, NETs, and fibrin also was observed in these patients compared with controls (Figure 12*H*), suggesting that FGL2 indeed mediated NETs formation and subsequent fibrin deposition and immune injury in HBV ALF.

Discussion

ALF is a fatal disease because of the aggressive progression and high mortality rate. To date, viral infections (hepatitis A, B, and E) still remain the predominant cause of ALF in developing countries.[35] However, the pathogenesis of FVH is not well known. It has been shown that innate immune response plays a causative role in ALF rather than direct viral-induced liver necrosis.[22] Existing studies have focused on macrophages and NK cells, however, little is known about the whole picture of the hepatic immune cell niche in viral-induced ALF.

In our study, we used a MHV-3–infected mouse model, which is considered a suitable model for studying the mechanism underlying FVH.[14] The single-cell RNA-seq showed that neutrophils were the only innate immune cell showing a significant increase in liver at 60 hours after MHV-3 infection, when the mice had severe systemic inflammation. Consistently, we detected gradually increased neutrophil infiltration in liver by immunohistochemical analysis after viral infection. Although other immune cells, such as T cells, macrophages, and NK cells, are implicated in the pathogenesis of viral hepatitis,[14,36–38] the role of neutrophils in host defense and disease progression in response to viral hepatitis has not been addressed thoroughly. In this study, the single-cell RNA-seq analysis showed that neutrophils were the cells with the most obvious change in number after MHV-3 infection. Moreover, the NETs formation pathway, which is associated closely with neutrophil function, was enriched in the Kyoto Encyclopedia of Genes and Genomes enrichment. Therefore, we attempted to investigate the role of NETs in the pathogenesis of FVH.

Increasing evidence has supported the contribution of NETs to the systemic inflammation and pathologic changes in ALF.[12] A very recent study from von Meijenfeldt et al[13] also showed that an increased level of NETs was associated with poor outcome in patients with ALF. Notably, compared with APAP-caused ALF, MPO-DNA levels were found to be higher in patients with ALF caused by non-APAP factors (virus, autoimmune, drugs, and so forth), suggesting that NETs might play different roles in ALF owing to different etiologies.[13] Consistently, abundant hepatic NETs formation and increased serum MPO DNA was observed in MHV-3–induced ALF, while NETs formation barely was observed either in vivo or in vitro after APAP treatment. In APAP-induced ALF, direct toxicity of APAP promoted hepatocyte death and damage associated molecular patterns (DAMPs) release, which then activated the innate immune system and induced an inflammatory response.[39,40] In viral-induced ALF, the innate immune system reacts immediately upon virus infection, thus an immune-mediated inflammatory response plays a much more important role in acute viral infection.[14,41]

Nevertheless, studies on mechanisms to investigate the role of NETs in the disease progression of viral-induced ALF still is lacking. Recent studies have shown that NETs act as a link between inflammation and coagulation. On the one hand, NETs contribute to inflammation through direct cell damage by histone and NE.[42,43] On the other hand, NETs also serve as a scaffold for fibrin deposition in thrombus formation.[7] Here, in MHV-3–infected mice, we observed not only enhanced NETs generation in liver and peripheral blood, but also co-localization of NETs and fibrin in the

Figure 7. (***See previous page***). **Neutrophil-specific FGL2 enhanced NETs formation and aggravated liver injury in MHV-3–infected mice.** (*A–D*) *Fgl2*$^{-/-}$ and WT mice were challenged with 100 plaque forming unit (PFU) of MHV-3. (*A*) H&E staining of liver tissue was shown at 24, 48, and 72 hours after MHV-3 injection (n = 5 in each group). *Arrows* indicate necrotic areas. (*B*) Representative images of liver tissues were shown at 72 hours after MHV-3 infection. (*C*) Serum ALT, AST, (*D*) TNF-α, IL1β, and IL6 levels were measured at the indicated time points after MHV-3 infection (n = 5 in each group). (E) *Fgl2*$^{-/-}$ or WT BM neutrophils were adoptively transferred intravenously into *fgl2*$^{-/-}$ mice as the time shaft indicated (n = 5 in each group). (*F*) Hepatic neutrophil infiltration after the adoptive transfer experiment were detected using immunochemistry. (*G*) Histologic liver tissues at 48 hours after MHV-3 injection were observed. (*H*) Serum ALT, AST, (*I*) TNF-α, IL1β, IL6, and (*J*) MPO-DNA levels (n = 5 in each group) were measured at 48 hours after MHV-3 infection. (*K*) Hepatic NETs formation was detected by immunofluorescence staining as previously described. (*L*) Fibrin deposition of liver tissues at 48 hours after MHV-3 injection was measured by immunohistochemistry. *Scale bars*: 50 μm. For immunochemical analysis, 10 microscopic fields per liver section from 3 mice in each group were counted using ImageJ. *$P < .05$, **$P < .01$, ***$P < .001$, and ****$P < .0001$, determined by 1-way analysis of variance.

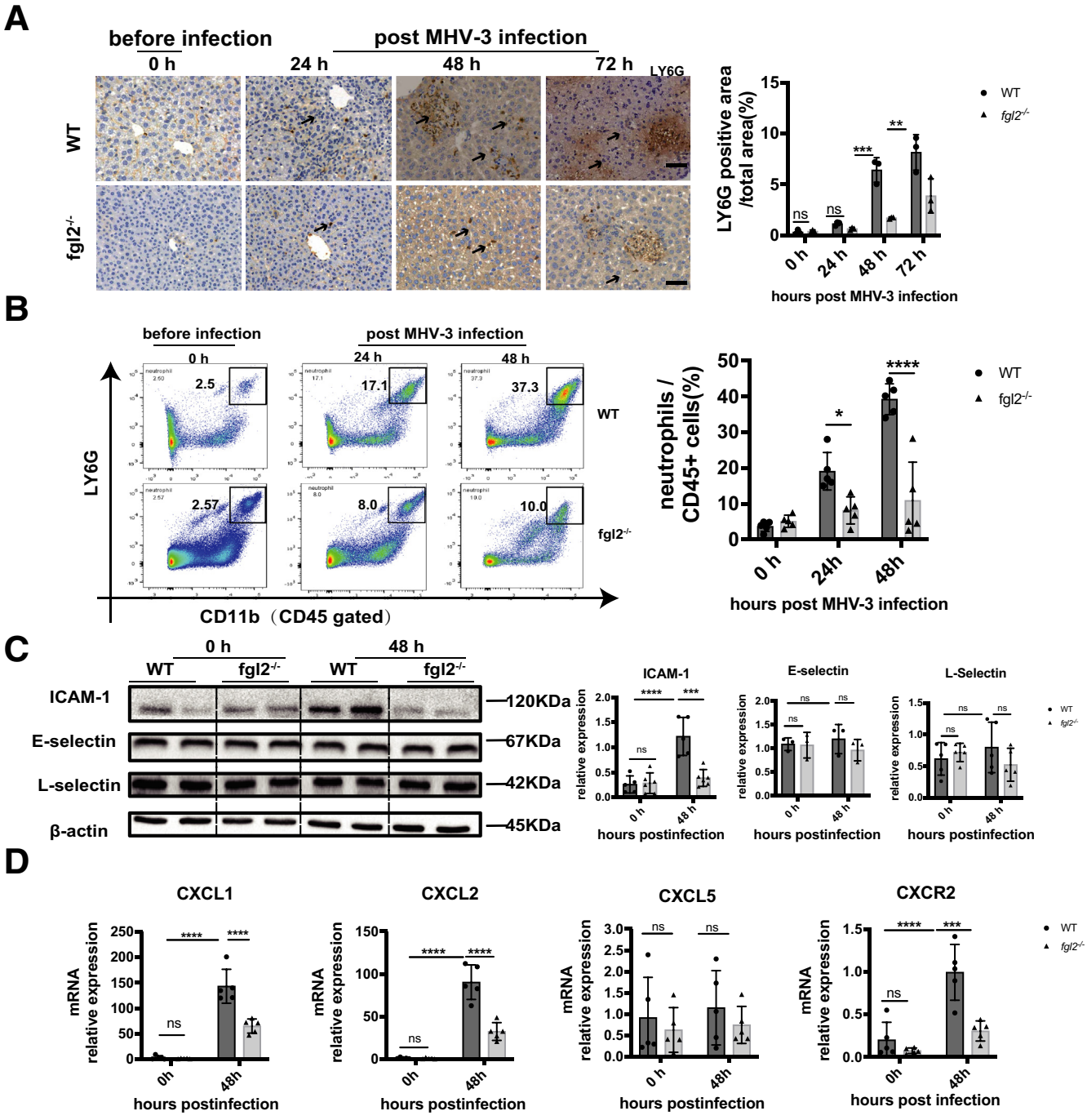

Figure 8. FGL2 promoted accumulation of hepatic neutrophils via enhanced expression of ICAM-1, *Cxcl1/2*, and *Cxcr2* in MHV-3 infection. Liver neutrophil infiltration was detected by Ly6G staining using (*A*) immunohistochemistry and (*B*) flow cytometry gated by CD45+CD11b+LY6G+. *Scale bars*: 50 μm. (*C*) Protein levels of hepatic ICAM-1, E-selectin, and L-selectin were measured by Western blot and analyzed by Image lab. (*D*) Relative mRNA levels of *Cxcl1*, *Cxcl2*, *Cxcl5*, and *Cxcr2* in liver were measured by quantitative reverse-transcription polymerase chain reaction and expressed as a ratio to β*-actin*. For bar graphs, n = 5 in each group. **P* < .05, ***P* < .01, ****P* < .001, and *****P* < .0001, determined by 1-way analysis of variance followed by the Tukey follow-up test. CXCL, Chemokine (C-X-C Motif) Ligand; CXCR, CXC chemokine receptor.

livers. Moreover, NETs depletion remarkably reduced hepatic fibrin deposition, coagulation activation, and inflammatory response, and consequently improved liver injury as well as survival rate in the murine model. Taken together, we show that NETs might accelerate the progression of FVH by promoting the inflammatory response and fibrin deposition.

A number of studies have indicated that FGL2-mediated microthrombosis and the inflammatory response is crucial for the pathogenesis of FVH.[4,14] To date, studies on FGL2

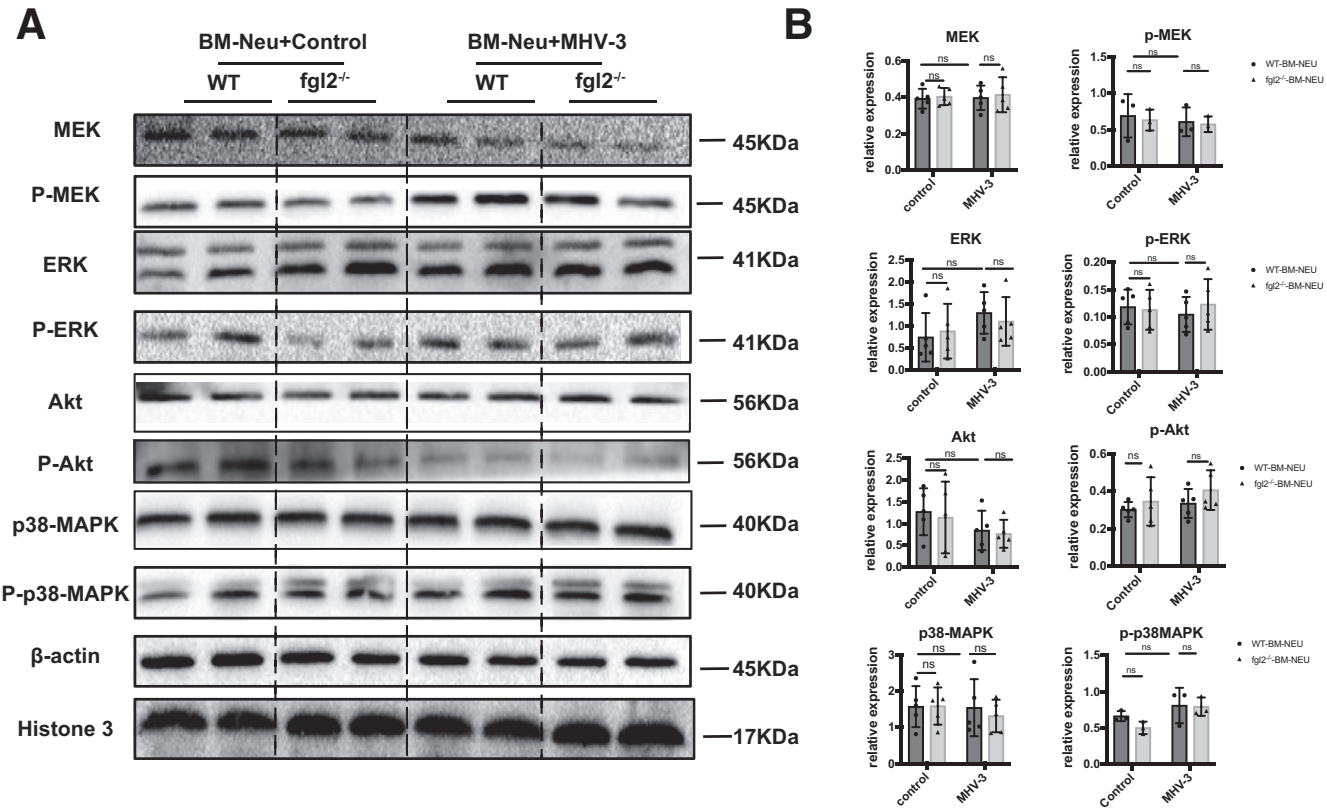

Figure 9. FGL2-mediated NETs formation is not determined by MEK/extracellular regulated protein kinase (ERK)/p38-mitogen-activated protein kinase (MAPK) after MHV-3 stimulation. (*A*) Isolated BM neutrophils of WT and *fgl2*$^{-/-}$ neutrophils were stimulated with MHV-3 or not in vitro. MEK, ERK, p38-MAPK, and Akt expression levels and their phosphorylated form were detected by Western blot. (*B*) Image density of these proteins was analyzed by Image Lab. For bar graphs, n = 3–5 in each group. Statistical analysis was performed by 1-way analysis of variance followed by the Tukey follow-up test. p-Akt, phospho-AKT; P-ERK, phospho-extracellular regulated protein kinase; P-MEK, phospho-Mitogen-activated Extracellular signal-regulated Kinase; p38, P38-Mitogen-Activated Protein Kinase.

were related mostly to macrophages and endothelial cells.[21] Interestingly, we observed increased membrane FGL2 expression on neutrophils after MHV-3 infection, which has not been focused on previously. Whole-transcriptome sequencing of liver leukocytes further showed a significantly down-regulated pathway of NETs formation upon FGL2 deficiency, implicating that FGL2 might be involved in the process of NETs formation. Through in vivo and in vitro experiments, we verified that both hepatic and BM fgl2-deficient neutrophils showed a decreased ability of NETs generation after MHV-3 infection compared with WT neutrophils. Moreover, adoptive transfer of WT neutrophils into *fgl2*$^{-/-}$ mice boosted NETs formation, increased hepatic fibrin deposition, and aggravated inflammatory injury in the recipient mice, whereas adoptive transfer of fgl2-deficient neutrophils showed no such effects. This result suggested the specific effect of neutrophil-expressed FGL2 in exacerbation of viral-induced liver injury. In addition to the modulation on NETs release, we found that FGL2 also facilitated neutrophil infiltration because FGL2 deficiency reduced expression of *Cxcl1/2*, *Cxcr2*, and adhesion molecular ICAM-1 in liver. This suggested that FGL2 increased the level of NETs in liver not only by directly inducing NETs generation but also by promoting neutrophil recruitment to the liver.

More interestingly, we discovered the colocalization of NETs, fibrin, and FGL2 in the liver of MHV-3–infected WT mice, but not in *fgl2*$^{-/-}$ mice. A potential mechanism might be that NETs provided a scaffold for the adhesion of increased dissociative membrane FGL2, which further promoted fibrin deposition and thrombosis. NETs were more like an effect amplifier for coagulation in this process owing to their enlarged area. This might be a novel pathway through which FGL2 contributed to coagulation, but further studies still are needed to reveal the in-depth mechanism.

Next, we attempted to explore the mechanism by which FGL2 mediated NETs formation. At present, the widely recognized pathways of NETs formation include MEK/extracellular regulated protein kinase, mitogen-activated protein kinase, and autophagy,[29] which all were examined in our study in the BM neutrophils under MHV-3 stimulation. Among these pathways, we only found a significant down-regulation of autophagy upon FGL2 deficiency. Autophagy is the major intracellular degradation system by which cytoplasmic materials are delivered to and degraded in the lysosome,[44] NETs and autophagy were considered to

be independent from each other until Remijsen et al[31] showed that autophagy and superoxide production both are needed for NETs formation. Angelidou et al[30] also discovered that the autophagy-driven NETs were involved in ulcerative colitis. To verify the regulatory effect of FGL2 on autophagy-driven NETs formation, we blocked

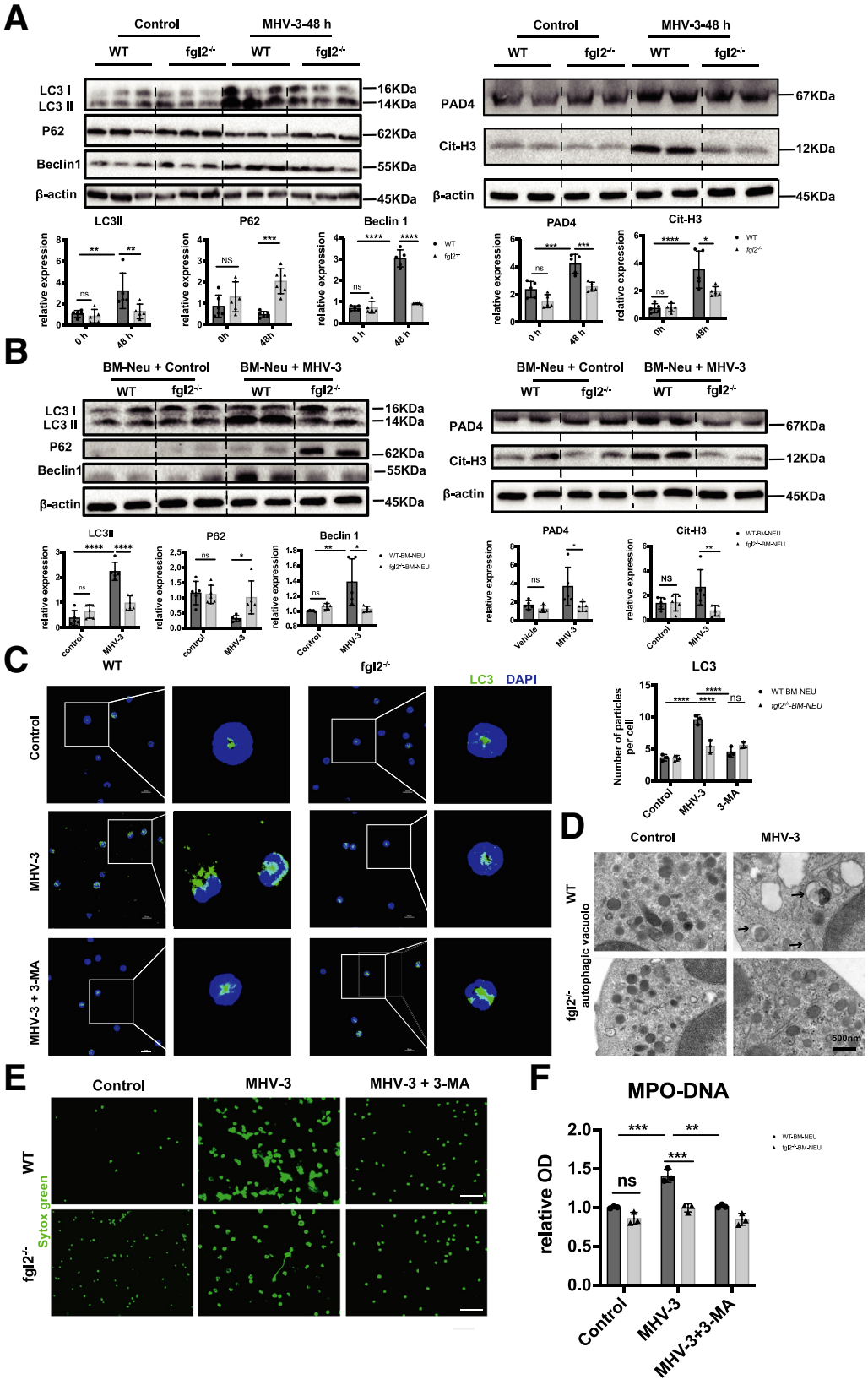

autophagy using 3-MA, which abolished the difference in MHV-3–induced NETs formation between WT and *fgl2*$^{-/-}$ neutrophils, implying that FGL2 indeed regulated induction of autophagy, which further mediated generation of NETs.

After that, we sought to elucidate the upstream signaling pathway through which FGL2 regulated autophagy. We used the STRING database to predict proteins that might interact with FGL2 and found that MCOLN3 is a possible target. MCOLN3, also called transient receptor potential channels 3 (TRPML3), is an inward-rectifying Ca^{2+} channel expressed in the plasma membrane and multiple intracellular compartments.[33] Recent studies have shown that MCOLN3 dynamically moves to subcellular sites for autophagosome formation where it may provide Ca^{2+} for the fusion process.[34] Moreover, the trafficking and channel function of MCOLN3 is regulated in the context of autophagy.[45] In line with the prediction, immunoprecipitation showed a direct interaction of FGL2 with MCOLN3, which was supported further by colocalization of MCOLN3 and FGL2 in MHV-3–infected neutrophils. Furthermore, treatment of MCOLN3 antibody on neutrophils inhibited MHV-3–induced calcium influx along with formation of autophagosomes and NETs. On the contrary, treatment of ML-SA1, an MCOLN3 agonist, reversed the negative effect of FGL2 deficiency on calcium influx, autophagy induction, and subsequent NETs formation. Therefore, the earlier-described findings showed that FGL2 contributed to NETs formation through the Ca^{2+} channel MCOLN3-mediated autophagy in neutrophils after MHV-3 infection.

Clinically, HBV remains a most frequent cause of viral-induced ALF worldwide. Both acute HBV infection and acute exacerbation of chronic HBV infection can result in ALI or ALF.[35] Therefore, we sought to verify the role of NETs in patients with HBV ALI/ALF. As expected, plasma MPO and MPO-DNA levels, which indicated NETs release, were higher in patients with HBV ALI/ALF than in controls (CHB and HC). More than that, an increased plasma MPO level was found to be associated with reduced prothrombin time activity and increased INR and TAT, suggesting the close correlation of NETs and disease severity. Consistent with increased NETs release, we observed higher mRNA levels of *FGL2* on peripheral neutrophils in patients with HBV ALI/ALF than in controls. More importantly, NETs mostly were released by FGL2+ neutrophils other than FGL2- neutrophils. The co-localization of hepatic NETs, FGL2, and fibrin in patients with HBV ALF further supported the hypothesis that FGL2 might participate in NETs-induced fibrin deposition. In short, these data suggest that FGL2-mediated NETs formation might aggravate disease progression through dysregulated coagulation in HBV ALI/ALF.

In conclusion, our results provide both experimental and clinical evidence that NETs contribute to hepatic fibrin deposition and inflammatory injury, which exacerbates disease progression in viral-induced ALF. Furthermore, we elucidated that the neutrophil-specific FGL2 promoted NETs formation through interaction with MCOLN3, which initiated autophagy by mediating calcium influx into the cell. Therefore, our study showed a novel mechanism for regulation of NETs formation, targeting NETs and FGL2 may provide a new strategy for the treatment of FVH.

Materials and Methods

Mice

C57BL/6 WT mice were purchased from Beijing Vital River Laboratory Animal Technology, Co, Ltd (Beijing, China). *Fgl2*$^{-/-}$ mice on a C57BL/6J background were constructed by Shanghai Model Organisms Center, Inc (Shanghai, China). Female WT littermates between 6 and 8 weeks old were used as controls. Mice were maintained in a specific pathogen-free environment at the Animal Experiment Center of Tongji Hospital, following the procedures approved by the Tongji Hospital Animal Ethics Committee (TJH-201802001).

Animal Treatment

A total of 100 plaque forming unit (PFU) of MHV-3 was injected intraperitoneally into the mice to establish a FVH model. MHV-3 was obtained from the American Type Culture Collection (Manassas, VA) and expanded according to a previously published protocol.[14] APAP (500 mg/kg) was used to establish a mouse model of non–virus-caused ALF. NETs were depleted by intraperitoneal injection of DNase I (750 U), a widely used method to remove the DNA scaffold of NETs,[8] at 4 hours and 48 hours after MHV-3 infection. For neutrophil depletion, mice were injected intraperitoneally with anti-Ly6G (clone 1A8; BioXcell, West Lebanon, NH) and rat IgG2a (clone 2A3; BioXcell, West Lebanon, NH) were used as an isotype control. To adoptively transfer neutrophils, BM neutrophils were purified using the Neutrophil Isolation Kit (Miltenyi Biotec, San Diego, CA). A total of 4×10^6 WT or *fgl2*$^{-/-}$ neutrophils were adoptively transferred into MHV-3–infected *fgl2*$^{-/-}$ mice by intravenous injection.

Figure 10. (***See previous page***). **FGL2 promoted NETs formation by induction of autophagy after MHV-3 challenge.** LC3, P62, Beclin 1 (*left panel*), PAD4, and Cit-H3 (*right panel*) expression levels in (*A*) hepatic tissues and (*B*) MHV-3–stimulated BM neutrophils were detected by Western blot and quantified by Image Lab (n = 5 in each group). (*C*) Autophagosome formation was detected by fluorescent staining of LC3 in the presence of autophagy inhibitor (3-MA) or not. *Scale bars*: 10 μm. The numbers of LC3 particles were counted in 3–5 microscopic fields per slide from 3 slides in each group. (*D*) Transmission electron microscopy images showed the presence of double-membrane autophagosomes (*arrowheads*) in isolated neutrophils. *Scale bars*: 500 nm. (*E*) BM neutrophils were treated with MHV-3 in the presence of 3-MA or not. The induction of NETs was measured by fluorescent microscopy using Sytox Green. (*F*) MPO-DNA levels in the supernatant were detected. n = 3 in each group. **P* < .05, ***P* < .01, ****P* < .001, and *****P* < .0001, determined by 1-way analysis of variance. DAPI, 4′,6-diamidino-2-phenylindole; OD, optical density.

Patient Sample Collection

We enrolled 23 patients with HBV ALI, 5 patients with HBV ALF, 45 patients with CHB, and 45 HCs. General information regarding these individuals is summarized in Table 1. HBV ALI was defined as an INR $\geq$ 1.5 with previous asymptomatic hepatitis B infection but in the absence of

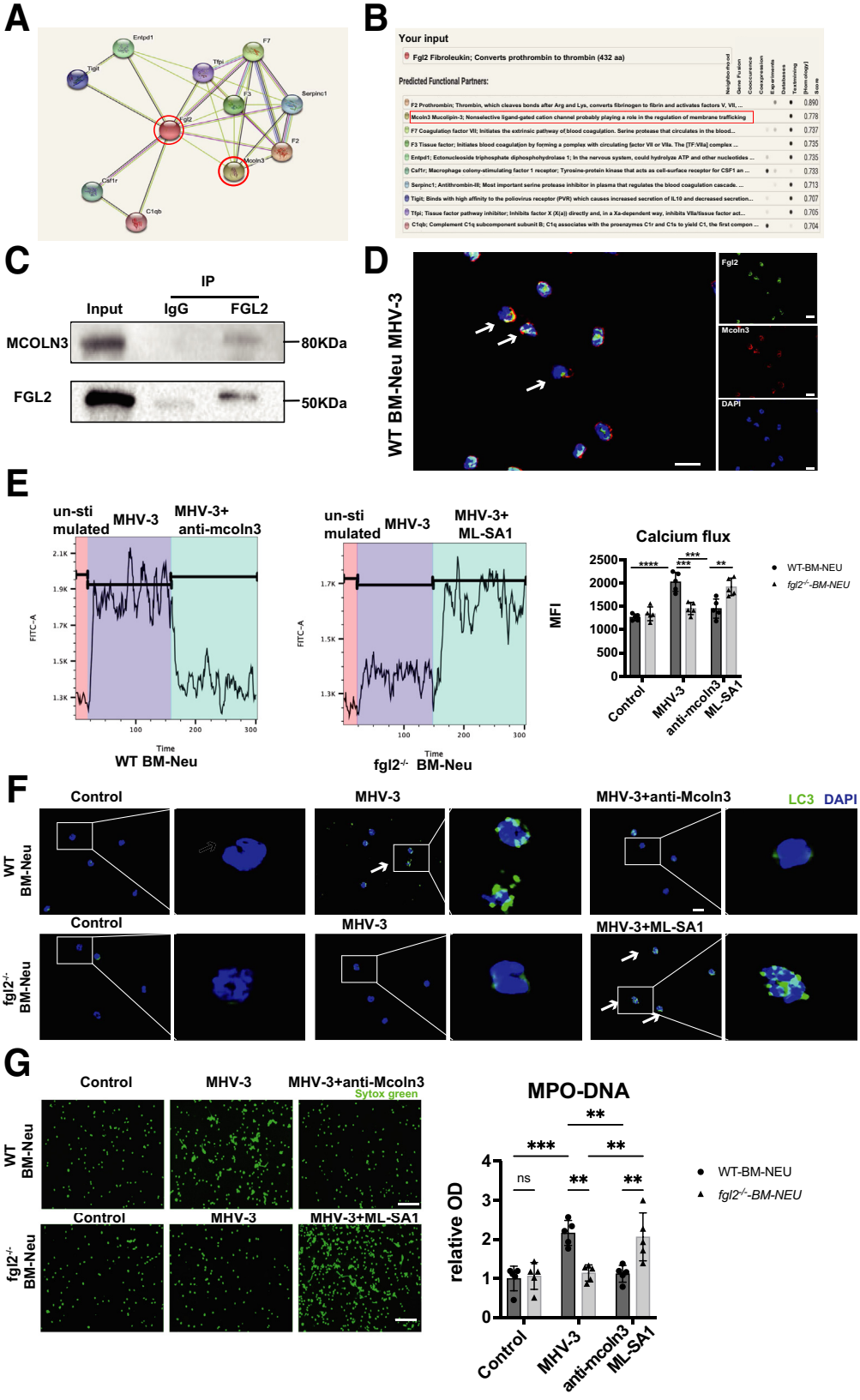

cirrhosis. HBV ALF was diagnosed similar to HBV ALI but with hepatic encephalopathy. These patients met the diagnosis criteria of ALI/ALF according to the European Association for the Study of the Liver guideline,[46] as well as the diagnosis criteria of acute on chronic liver failure according to the Asian Pacific Association for the Study of the Liver guideline.[47] Plasma and peripheral whole blood were obtained from the earlier-described 3 groups to detect NETs-related factors. Liver samples were obtained from 5 patients with HBV ALF who underwent liver transplantation. Human liver samples with benign hepatic hemangioma were used as controls. The liver samples were immediately fixed or frozen for all experiments. All participants signed an informed consent for participation in this study. Human studies were approved by the local ethics committee of Tongji Hospital, Tongji Medical College, Huazhong University of Science and Technology (2021S125).

Liver Leukocytes Preparation

Liver leukocytes were isolated according to a previously described method.[48] In brief, liver tissues were digested with collagenase IV first. After filtering through a 100-μm cell strainer, the resulting cell pellet was resuspended in 10 mL of 35% Percoll. The leukocytes harvested by density gradient centrifugation then were resuspended in 5 mL of red blood cell lysis buffer. All procedures were conducted carefully and quickly on ice under sterile condition to ensure cell viability and avoid cell activation. The cell was used for single-cell RNA-seq, whole transcriptome sequencing, and flow cytometry.

Single-Cell RNA-Seq

Liver leukocytes were isolated from MHV-3–infected (60 hours) and uninfected mice. After a guarantee of cell viability (>90%), the cells underwent single-cell RNA-seq (NovaSeq 6000; Illumina, San Diego, CA). After quality control, data alignment, and sample aggravating, the cells were clustered into 8 groups.

Primary Neutrophil Isolation

BM neutrophils were isolated from WT and *fgl2*$^{-/-}$ mice as previously described.[49] Briefly, bone marrow cells of the femur and tibia were isolated by density gradient centrifugation using Histopaque 1119 (Sigma, St. Louis, MO) and Histopaque 1077 (Sigma, St. Louis, MO). The intermediate circle between Histopaque 119 and Histopaque 1077 was collected and purified using MACS microbeads (Miltenyi Biotec, San Diego, CA) following the manufacturer's instruction. All procedures were conducted carefully and quickly on ice under sterile condition to ensure cell viability and avoid cell activation. The purity of these neutrophils was more than 90%, as assessed by flow cytometry.

Blood neutrophils were isolated using previously published protocols.[50] Briefly, Histopaque 1119 gradient was used to remove red blood cells. Then, leukocytes were separated with a 65%–70%–75%–80%–85% Percoll gradient. Neutrophils were collected in fractions greater than 70%. Cells were washed twice with phosphate-buffered saline (PBS).

NETs Detection

The peripheral levels of NETs in patients and mice were evaluated by detection of MPO and MPO-DNA levels. MPO was detected using an enzyme-linked immunosorbent assay (ELISA) kit. MPO DNA was detected according to a previously described ELISA capture method.[51] In brief, 96-well microtiter plates precoated with MPO from the earlier-described ELISA kits were used. Plasma from patients or mouse serum was mixed with peroxidase-labeled anti-DNA monoclonal antibody (component 2 of the Cell Death Detection ELISA kit, Roche, Basel, Switzerland), incubated at room temperature for 2 hours, and washed by PBS 3 times. Then, peroxidase substrate was added for a 30-minute incubation at 37°C. The optical density was measured at 450 nm.

For in vitro study, 4×10^5 isolated neutrophils were seeded on coverslips precoated with polylysine and stimulated with MHV-3 (multiplicity of infection, 1) for 3 hours in 12-well microtiter plates. After stimulation, 5 μmol/L Sytox Green was added to the cells to detect extracellular DNA immediately.[8]

ELISA Measurements

The levels of TNF-a, IL1β, IL6, FGL2, and TAT of serum, plasma, or cell culture supernatant were detected using kits according to the manufacturer's instructions.

Co-immunoprecipitation

Liver leukocytes from 8 infected WT mice were pooled together and went for MACS separation using microbeads

Figure 11. (***See previous page***). **FGL2 induced autophagy through interaction with MCOLN3 after MHV-3 infection.** (*A*) FGL2-centered protein interaction prediction network using the STRING database. (*B*) The top 10 FGL2-regulated proteins and FGL2-MCOLN3 interaction analysis. (*C*) Co-immunoprecipitation of the interaction between FGL2 and MCOLN3. Neutrophil lysates isolated from livers of 8 WT mice were immunoprecipitated with an anti-FGL2 monoclonal antibody. (*D*) Neutrophils isolated from WT mice were stimulated with MHV-3 in vitro. The colocalization of MCOLN3 and FGL2 were detected by immunofluorescence microscopy (*arrowheads*). *Scale bars*: 10 μm. (*E*) WT or *fgl2*$^{-/-}$ BM neutrophils were preincubated with MHV-3, organellar Ca^{2+} efflux was measured by applying 20 μmol/L ML-SA1 and anti-MCOLN3 antibody. (*F* and *G*) BM neutrophils were preincubated with anti-MCOLN3 (1 μg/mL) or ML-SA1 (20 μmol/L), and then stimulated with MHV-3 for 3 hours. (*F*) Autophagosome formation was detected by LC3 fluorescent staining. The arrowhead indicated LC3 puncta cells. *Scale bars*: 10 μm. (*G*) NETs formation was detected by fluorescent staining with Sytox Green. *Scale bars*: 50 μm. MPO-DNA levels in the supernatant were detected and are shown (*right*). n = 5 in each group. $^{**}P < .01$, $^{***}P < .001$, and $^{****}P < .0001$, determined by 1-way analysis of variance. DAPI, 4′,6-diamidino-2-phenylindole; IP, immunoprecipitation.

following the manufacturer's instruction to ensure the purity. Total proteins were extracted by cell lysis buffer immunoprecipitation. After precleaning with Protein A/G Magnetic beads, the proteins were incubated with fgl2 antibody in eppendorf tubes at 4°C overnight. Then, the lysate and antibody solution were transferred into a tube

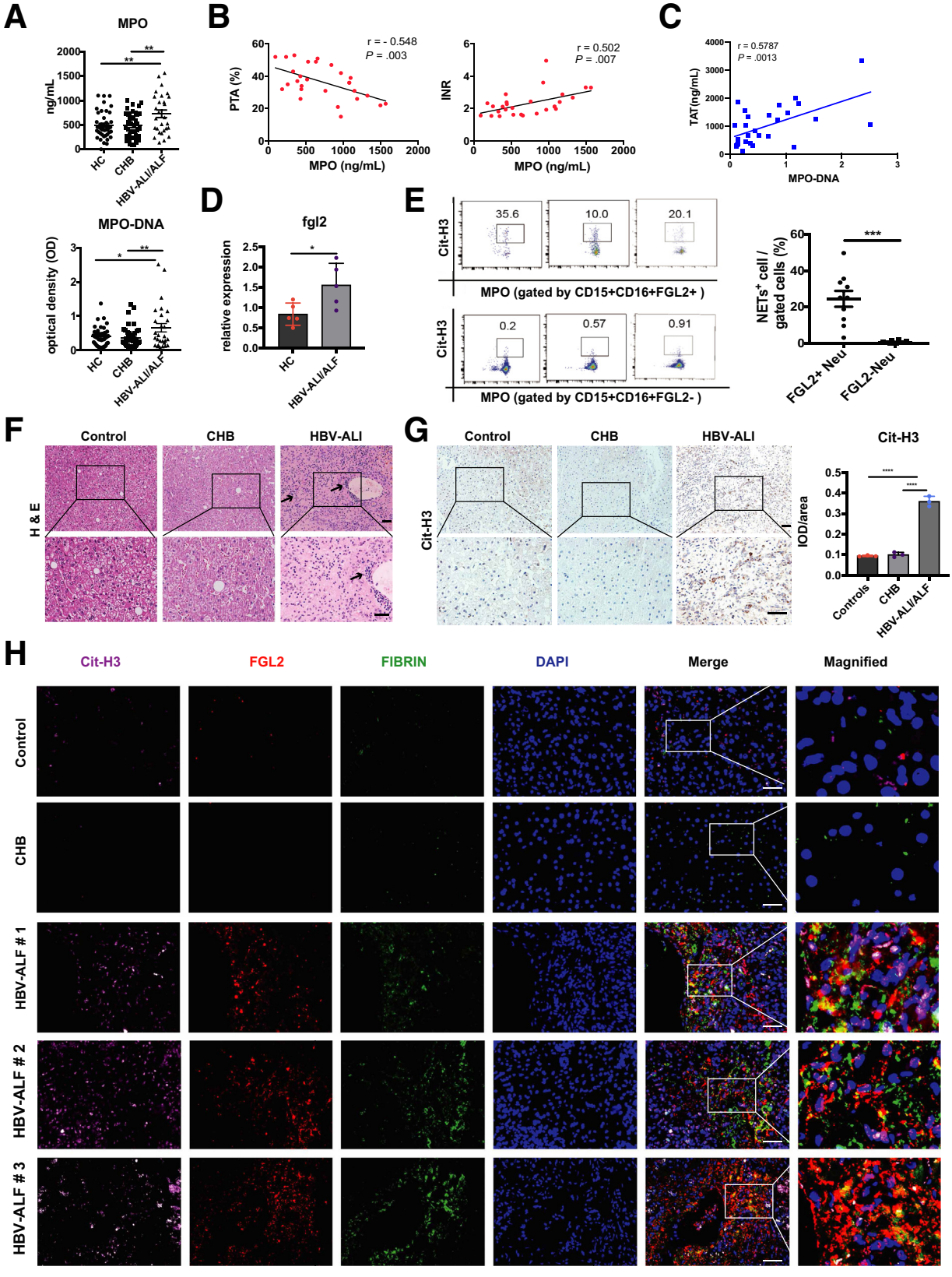

Table 1. Baseline Characteristics of Study Population

Variables	HC (n = 45)	CHB (n = 45)	HBV-ALI (n = 28)	HC vs CHB, P value	HC vs HBV-ALI, P value		HBV-ALI vs CHB, P value
Age, y	43 ± 15	39 ± 10		44 ± 12	.6626	>.9999	.42
Male, %	80	75.56		92.86	.6121	.1354	.06
Viral							
HBV-DNA positive, %	-	24.44		96.43	-	-	<.01
HBV DNA, Lg10, IU/ mL	-	2 (1.3–2.3)		6.02 (4.73–7.18)	-	-	<.01
HBeAg positivity, %	-	17.78		21.43	-	-	.81
Laboratory values on admission							
ALT, U/L	17 (12–22)	22 (16–34)		185.5 (64.75–510)	.66	<.01	<.01
Albumin, g/L	47.61 ± 2.02	47.1 (46.35–48.35)		33.35 (30.4–37.6)	>.99	<.01	<.01
Serum bilirubin, μmol/L	26.85 (23.88–28.78)	21.6 (9.25–48.65)		302.543 ± 129.7	<.01	<.01	<.01
Neu (#)	3.52 ± 1.18	3.13 ± 0.99		4.69 (3.16–6.08)	.84	.02	.02
Platelet count, 10^9/L	230.85 ± 49.70	194.2 ± 61.27		114.07 ± 67.1	.48	<.01	.02
INR	-	-		2.32 ± 0.77	-	-	-
MELD score	-	-		24.48 ± 5.93	-	-	-

NOTE. Data are expressed as means ± SD (normal distribution), medians (interquartile range) (abnormal distribution), or number (%). Comparisons between cohorts were performed with the Mann–Whitney *U* test or the chi-square test.
HBeAg, hepatitis B e antigen; MELD, model for end-stage liver disease.

containing prewashed magnetic bead pellet. After incubating with rotation for 4 hours at 4°C, the pellet beads were collected and heated at 100°C for 8 minutes with lysis buffer. Then, the lysis buffer was validated by Western blot. Fgl2 antibody and MCOLN3 polyclonal antibody were used as target antibodies. Mouse (G3A1) monoclonal antibody IgG1 isotype control were used as control antibodies.

Measurement of Calcium Influx

BM neutrophils were loaded with 0.5 μmol/L Fura-4 AM for 30 minutes at 37°C. The cells then were perfused continuously with the indicated stimulations. Finally, the calcium flux was measured at fluorescein isothiocyanate (FITC) channel using flowcytometry.

Antibodies and Reagents

The antibodies used for immunohistochemistry, immunofluorescence, Western blot, and flow cytometry in this study are listed in Table 2. The reagents used for this experiment are provided in Table 3.

Confocal Microscopy

Purified BM neutrophils cultured in 1640 RPMI medium were plated on poly-l-lysine–coated coverslips in a 12-well culture plate and left for 30 minutes to adhere. Adherent cells were incubated with MHV-3 or vehicle for 3 hours, additional autophagy inhibitor 3-methyladenine was added or not. After incubation, the cells were fixed using 4% cold paraformaldehyde for 10 minutes, permeabilized with PBS and 0.1% Triton X-100, 1% goat serum plus 5% bovine serum albumin, and stained with antibodies against LC3. Images were acquired with a NIKON (Tokyo, Japan) Eclipse Ti confocal microscope.

Transmission Electron Microscopy

After different stimulations, isolated neutrophils were collected and washed 3 times, the pellets were fixed in 1% osmium tetroxide in cacodylate buffer for 1 hour, dehydrated through a graded series of acetone, and embedded in epoxy-based resin. The sections were observed in a Hitachi (Tokyo, Japan) H7650 transmission electron microscope, and images were taken with an AMT (Danvers, MA) 16000 digital camera mounted on the microscope.

Figure 12. (***See previous page***). **FGL2 expression is associated with NETs release and fibrin deposition in patients with HBV ALI/ALF.** (*A*) Plasma from patients with HBV ALI/ALF (n = 28) or with CHB (n = 45) or HCs (n = 45) was assessed for MPO and MPO-DNA levels. (*B*) Correlation between MPO levels with prothrombin time activity (PTA) and INR was evaluated in the patients with HBV ALI/ALF. (*C*) Correlation between MPO-DNA levels with TAT was evaluated in patients with HBV ALI/ALF. (*D*) mRNA levels of *FGL2* expression on peripheral neutrophils were detected in patients with HBV ALI/ALF and HCs. (*E*) NETs expression in FGL2+ neutrophils or FGL2- neutrophils from patients with HBV ALI was examined using flow cytometry (n = 10 in each group). In patients with HBV ALF and controls, (*F*) H&E staining showed liver damage, and (*G*) immunochemistry staining of Cit-H3 showed hepatic NETs formation quantified by ImageJ. (*H*) Representative immunofluorescence staining of FGL2 (red), Cit-H3 (pink), and fibrin (green) staining in liver. *Scale bars*: 50 μm. *$P < .05$, **$P < .01$, ***$P < .001$, and ****$P < .0001$, determined by 1-way analysis of variance. DAPI, 4′,6-diamidino-2-phenylindole.

Table 2. Antibodies Used in This Study

Antibodies	Company	Cat. no.
Anti-neutrophil elastase	Abcam (Cambridge, MA)	ab68672
Anti–histone H3 (citrulline R2 + R8 + R17)	Abcam (Cambridge, MA)	ab5103
Antifibrinogen	Abcam (Cambridge, MA)	ab34269
Anti-LY6G	Abcam (Cambridge, MA)	ab238132
MPO antibody	Abcam (Cambridge, MA)	ab25989
Anti-p38 MAPK	CST (Danvers, MA)	8690S
Anti-P62	CST (Danvers, MA)	8025S
Anti–beclin-1	CST (Danvers, MA)	3738S
Anti-LC3	CST (Danvers, MA)	12741S
Anti-MEK1/2	CST (Danvers, MA)	4694S
Mouse (G3A1) monoclonal antibody IgG1 isotype control	CST (Danvers, MA)	5415S
Anti–phospho-MEK1/2	CST (Danvers, MA)	9154S
Anti–phospho-p38-MAPK	CST (Danvers, MA)	4511S
Anti–phospho-p44/42 MAPK (Erk1/2)	CST (Danvers, MA)	4370S
Anti–β-actin	CST (Danvers, MA)	4970S
Anti-Akt	Proteintech (Rosemont, IL)	10176-2-AP
Anti-ERK1/2	Proteintech (Rosemont, IL)	16443-1-AP
Anti–E-selectin	Proteintech (Rosemont, IL)	20894-1-AP
Anti–ICAM-1	Proteintech (Rosemont, IL)	10831-1-AP
Anti-MCOLN3	Proteintech (Rosemont, IL)	13879-1-AP
Anti-PAD4	Proteintech (Rosemont, IL)	17373-1-AP
Anti–phospho-Akt	Proteintech (Rosemont, IL)	66444-1-Ig
Fgl2 antibody	Abnova (Taiwan, China)	H00010875-M01
Anti–L-selectin	BOSTER (Wuhan, China)	PB9389
Anti-Ly6G antibody (1A8)	BioXCell (West Lebanon, NH)	BP0075-1
Anti-mouse CD16/32	BioLegend (San Diego, CA)	101302
Percp/Cyanine 5.5 anti-mouse Ly-6G	BioLegend (San Diego, CA)	27616
FITC anti-mouse CD45	BioLegend (San Diego, CA)	103108
APC anti-mouse/human CD11b	BioLegend (San Diego, CA)	101212
APC-Cy7 tandem-labeled goat anti-rabbit IgG (H+L)	AAT Bioquest (Sunnyvale, California)	16873
BD horizon bb515 mouse anti-human cd15	BD (Lexington, KY)	565236
BD Pharmingen pe-cy 7 mouse anti-human cd16	BD (Lexington, KY)	560716
Fixable viability stain 780	BD (Lexington, KY)	565388
APC anti-human fgl2	LSBio (Seattle, WA)	LS-C214244

ERK, extracellular regulated protein kinase; FITC, fluorescein isothiocyanate; H+L, heavy chain and light chain; MAPK, mitogen-activated protein kinase; MEK, Mitogen-activated Extracellular signal-regulated Kinase.

Quantitative Polymerase Chain Reaction

Total RNA was extracted from liver tissues using TRIzol reagent (Invitrogen, Carlsbad, CA). A total of 1 μg of total RNA was reverse-transcribed to complementary DNA using the ReverTraAce@qPCR RT kit (TOYOBO, Osaka, Japan) according to the manufacturer's instructions. The expression of target genes was detected by a real-time polymerase chain reaction system (CXF96; Bio-Rad, Hercules, CA) using SYBR Green Real-Time Polymerase Chain Reaction Master Mix (TOYOBO, Osaka, Japan). The primer sequences are shown in Table 4. Relative gene expression was analyzed by the $2^{-\Delta\Delta \text{Cycle Threshold}}$ method.

Western Blot Analysis

Liver tissues and cells were lysed using RIPA lysis buffer (AR0102; BOSTER, Wuhan, China) mixed with broad-spectrum protease inhibitor (AR1194; BOSTER) and phosphatase inhibitor (AR1195; BOSTER). After incubation with the lysis buffer for 20 minutes, the lysates were sonicated and centrifuged at 25,000 $\times$ g for 10 minutes at 4°C. A total of 30 μg protein was subjected to polyacrylamide gels made by NewFlash Protein AnyKD PAGE (8012011; Dakewe Biotech, Shenzhen, China) and transferred to polyvinylidene difluoride membranes. Membranes were blocked with 5% milk in Tris-buffered saline Tween 20 (TBST) and incubated with primary antibodies

Table 3. Reagents Used in This Study

Reagents	Company	Cat. no.
Neutrophil isolation kit	Miltenyi Biotec (San Diego, CA)	130-097-658
Histopaque 1077	Sigma (St. Louis, MO)	RNBJ0383
Histopaque 1119	Sigma (St. Louis, MO)	RNBH9868
3-MA	Sigma (St. Louis, MO)	M9281
Human FGL2 ELISA kit	BioLegend (San Diego, CA)	436907
Human MPO ELISA kit	BioLegend (San Diego, CA)	440007
Human thrombin-antithrombin complex ELISA kit (TAT)	Abcam (Cambridge, MA)	ab108907
Mouse thrombin-antithrombin complex ELISA kit (TAT)	Abcam (Cambridge, MA)	ab137994
Mouse MPO ELISA kit	Invitrogen (Carlsbad, CA)	EMMPOX10
Sytox Green	Invitrogen (Carlsbad, CA)	S7020
TRIzol reagent	Invitrogen (Carlsbad, CA)	15596026
Apap	APExBIO (Houston, Texas)	B3532
Cell death detection ELISA kit	Roche (Basel, Switzerland)	1774425001
Horseradish peroxidase goat anti-mouse IgG	Abbkine (Wuhan, China)	A21010
TNF-α	Novus (Novus Littleton, CO)	VAL609
Il6	Novus (Novus Littleton, CO)	VAL604
IL1β	Novus (Novus Littleton, CO)	VAL601
Protein A/G magnetic beads	MedChemExpress	HYK0202
ML-SA1	MedChemExpress Monmouth Junction, NJ	HY-108462
Newflash protein anykd polyacrylamide gel electrophoresis	Dakewe Biotec	8012011
bicinchoninic acid (BCA) protein quantification kit	BOSTER (Wuhan, China)	AR1189
Collagenase IV	Solarbio (Beijing, China)	C8160
Cy3 conjugated donkey anti-mouse IgG (heavy chain and light chain)	Servicebio (Wuhan, China)	GB21401
Cy3 conjugated donkey anti-mouse IgG (heavy chain and light chain)	Servicebio (Wuhan, China)	GB21401
4′,6-diamidino-2-phenylindole	Servicebio (Wuhan, China)	G1012
DNase I	Solarbio (Beijing, China)	D8071
Fura-4 am	Beyotime (Shanghai, China)	S1060
Cell lysis buffer immunoprecipitation	Beyotime (Shanghai, China)	P0013
Revertraace@qpcr RT kit	TOYOBO (Osaka, Japan)	FSQ-101
SYBR Green Real-time PCR Master Mix	TOYOBO (Osaka, Japan)	QPK-201
Percoll	GE Healthcare (Chicago, IL)	17-0891-09
Red blood cell lysis buffer	BioFlux (Hangzhou, China)	BSA06M1

Table 4. mRNA Primer Sequences Used in This Study

Gene	Primer sequence
Mouse *Cxcl1*	Forward: 5'-ACTCAAGAATGGTCGCGAGG-3' Reverse: 5'-GTGCCATCAGAGCAGTCTGT-3'
Mouse *Cxcl2*	Forward: 5'-GCGCCCAGACAGAAGTCATA-3' Reverse: 5'-CGAGGCACATCAGGTACGAT-3'
Mouse *Cxcl5*	Forward: 5'-TTGTCCACAATGAGCCTCCA-3' Reverse: 5'-TCAGCCCTTTCTTCTCTTCACTG-3'
Mouse *Cxcr2*	Forward: 5'-ACAGCTACTTGGGAGGCTGA-3' Reverse: 5'-TGCAGTGGTCACACCATTTT-3'
Mouse *β-actin*	Forward: 5'-GGTCAGAAGGACTCCTATGTGG-3' Reverse: 5'-TGTCGTCCCAGTTGGTAACA-3'
Human *FGL2*	Forward: 5'-GGTGCTCAAAGAAGTGCGGA-3' Reverse: 5'-GTTCCTGGACTCTACTGTCCTC-3'
Human *GAPDH*	Forward: 5'-GGAGCGAGATCCCTCCAAAAT-3' Reverse: 5'-GGCTGTTGTCATACTTCTCATGG-3'

and secondary antibodies. Proteins were detected using an enhanced chemiluminescence system (ChemiDoc XRS+; Bio-Rad) and the integrated optical density of the proteins was calculated using Image Lab software. The dilution ratios of primary antibodies and secondary antibodies used here were 1:1000 and 1:10,000. The antibodies used here are listed in Table 2.

Statistical Analysis

All data are presented as means ± SD. Unpaired Student *t* tests were used for comparisons between 2 experimental groups when data conformed to a normal distribution and homogeneity of variance. The Mann–Whitney *U* test was used for non-normally distributed data. Data with a normal distribution and homogeneity of variance from multiple groups were compared using 1-way analysis of variance with Turkey correction.

The Spearman rank correlation coefficient analysis was applied to analyze the correlation between MPO/MPO-DNA expression and clinical indicators. The log-rank test was used to analyze the survival rate. Statistical significance was set at $P < .05$.

References

1. Stravitz RT, Lee WM. Acute liver failure. Lancet 2019; 394:869–881.
2. Jayakumar S, Chowdhury R, Ye C, Karvellas CJ. Fulminant viral hepatitis. Crit Care Clin 2013;29:677–697.
3. Xu GL, Chen J, Yang F, Li GQ, Zheng LX, Wu YZ. C5a/C5aR pathway is essential for the pathogenesis of murine viral fulminant hepatitis by way of potentiating Fgl2/fibroleukin expression. Hepatology 2014;60:114–124.
4. Yang C, Chen Y, Guo G, Li H, Cao D, Xu H, Guo S, Fei L, Yan W, Ning Q, Zheng L, Wu Y. Expression of B and T lymphocyte attenuator (BTLA) in macrophages contributes to the fulminant hepatitis caused by murine hepatitis virus strain-3. Gut 2013;62:1204–1213.
5. Rolando N, Wade J, Davalos M, Wendon J, Philpott-Howard J, Williams R. The systemic inflammatory response syndrome in acute liver failure. Hepatology 2000;32:734–739.
6. Ganey PE, Luyendyk JP, Newport SW, Eagle TM, Maddox JF, Mackman N, Roth RA. Role of the coagulation system in acetaminophen-induced hepatotoxicity in mice. Hepatology 2007;46:1177–1186.
7. Fuchs TA, Brill A, Duerschmied D, Schatzberg D, Monestier M, Myers DD Jr, Wrobleski SK, Wakefield TW, Hartwig JH, Wagner DD. Extracellular DNA traps promote thrombosis. Proc Natl Acad Sci U S A 2010; 107:15880–15885.
8. Brinkmann VRU, Goosmann C, Fauler B, Uhlemann Y, Weiss DS, Weinrauch Y, Zychlinsky A. Neutrophil extracellular traps kill bacteria. Science 2004; 303:1532–1535.
9. Jin L, Batra S, Jeyaseelan S. Diminished neutrophil extracellular trap (NET) formation is a novel innate immune deficiency induced by acute ethanol exposure in polymicrobial sepsis, which can be rescued by CXCL1. PLoS Pathog 2017;13:e1006637.
10. Brill A, Fuchs TA, Savchenko AS, Thomas GM, Martinod K, De Meyer SF, Bhandari AA, Wagner DD. Neutrophil extracellular traps promote deep vein thrombosis in mice. J Thromb Haemost 2012;10:136–144.
11. McDonald B, Davis RP, Kim SJ, Tse M, Esmon CT, Kolaczkowska E, Jenne CN. Platelets and neutrophil extracellular traps collaborate to promote intravascular coagulation during sepsis in mice. Blood 2017; 129:1357–1367.
12. Honda M, Kubes P. Neutrophils and neutrophil extracellular traps in the liver and gastrointestinal system. Nat Rev Gastroenterol Hepatol 2018;15:206–221.
13. von Meijenfeldt FA, Stravitz RT, Zhang J, Adelmeijer J, Zen Y, Durkalski V, Lee WM, Lisman T. Generation of neutrophil extracellular traps in patients with acute liver failure is associated with poor outcome. Hepatology 2022;75:623–633.
14. Marsden PA, Ning Q, Fung LS, Luo X, Chen Y, Mendicino M, Ghanekar A, Scott JA, Miller T, Chan CWY, Chan MWC, He W, Gorczynski RM, Grant DR, Clark DA, Phillips MJ, Levy GA. The Fgl2/fibroleukin prothrombinase contributes to immunologically mediated thrombosis in experimental and human viral hepatitis. J Clin Invest 2003;112:58–66.
15. Liu H, Shalev I, Manuel J, He W, Leung E, Crookshank J, Liu MF, Diao J, Cattral M, Clark DA, Isenman DE, Gorczynski RM, Grant DR, Zhang L, Phillips MJ, Cybulsky MI, Levy GA. The FGL2-FcγRIIB pathway: a novel mechanism leading to immunosuppression. Eur J Immunol 2008;38:3114–3126.
16. Chen T, Ye X, Huang Z, Chen R, Zhuge X, Chen X, Du Y. Fgl2 prothrombinase is involved in severe acute pancreatitis-associated liver injury. Hepatogastroenterology 2012;59:1225–1229.
17. Han M, Yan W, Huang Y, Yao H, Wang Z, Xi D, Li W, Zhou Y, Hou J, Luo X, Ning Q. The nucleocapsid protein of SARS-CoV induces transcription of hfgl2 prothrombinase gene dependent on C/EBP alpha. J Biochem 2008;144:51–62.
18. Ning Q, Sun Y, Han M, Zhang L, Zhu C, Zhang W, Guo H, Li J, Yan W, Gong F, Chen Z, He W, Koscik C, Smith R, Gorczynski R, Levy G, Luo X. Role of fibrinogen-like protein 2 prothrombinase/fibroleukin in experimental and human allograft rejection. J Immunol 2005;174:7403–7411.
19. Zhou Y, Lei J, Xie Q, Wu L, Jin S, Guo B, Wang X, Yan G, Zhang Q, Zhao H, Zhang J, Zhang X, Wang J, Gu J, Liu X, Ye D, Miao H, Serhan CN, Li Y. Fibrinogen-like protein 2 controls sepsis catabasis by interacting with resolvin Dp5. Sci Adv 2019;5:eaax0629.
20. Hu J, Wang H, Li X, Liu Y, Mi Y, Kong H, Xi D, Yan W, Luo X, Ning Q, Wang X. Fibrinogen-like protein 2 aggravates nonalcoholic steatohepatitis via interaction with TLR4, eliciting inflammation in macrophages and inducing hepatic lipid metabolism disorder. Theranostics 2020;10:9702–9720.
21. Hu J, Yan J, Rao G, Latha K, Overwijk WW, Heimberger AB, Li S. The duality of Fgl2 - secreted immune checkpoint regulator versus membrane-associated procoagulant: therapeutic potential and implications. Int Rev Immunol 2016;35:325–339.
22. Wang X, Ning Q. Immune mediated liver failure. EXCLI J 2014;13:1131–1144.
23. Iwasaki A, Pillai PS. Innate immunity to influenza virus infection. Nat Rev Immunol 2014;14:315–328.
24. Donkel SJ, Wolters FJ, Ikram MA, de Maat MPM. Circulating myeloperoxidase (MPO)-DNA complexes as marker for neutrophil extracellular traps (NETs) levels and the association with cardiovascular risk factors in the general population. PLoS One 2021;16: e0253698.
25. Wang Y, Li M, Stadler S, Correll S, Li P, Wang D, Hayama R, Leonelli L, Han H, Grigoryev SA, Allis CD, Coonrod SA. Histone hypercitrullination mediates chromatin decondensation and neutrophil extracellular trap formation. J Cell Biol 2009;184:205–213.
26. Jenne CN, Wong CH, Zemp FJ, McDonald B, Rahman MM, Forsyth PA, McFadden G, Kubes P.

Neutrophils recruited to sites of infection protect from virus challenge by releasing neutrophil extracellular traps. Cell Host Microbe 2013;13:169–180.
27. Galani IE, Andreakos E. Neutrophils in viral infections: current concepts and caveats. J Leukoc Biol 2015; 98:557–564.
28. Borregaard N. Neutrophils, from marrow to microbes. Immunity 2010;33:657–670.
29. Papayannopoulos V. Neutrophil extracellular traps in immunity and disease. Nat Rev Immunol 2018; 18:134–147.
30. Angelidou I, Chrysanthopoulou A, Mitsios A, Arelaki S, Arampatzioglou A, Kambas K, Ritis D, Tsironidou V, Moschos I, Dalla V, Stakos D, Kouklakis G, Mitroulis I, Ritis K, Skendros P. REDD1/autophagy pathway is associated with neutrophil-driven IL-1beta inflammatory response in active ulcerative colitis. J Immunol 2018; 200:3950–3961.
31. Remijsen Q, Vanden Berghe T, Wirawan E, Asselbergh B, Parthoens E, De Rycke R, Noppen S, Delforge M, Willems J, Vandenabeele P. Neutrophil extracellular trap cell death requires both autophagy and superoxide generation. Cell Res 2011;21:290–304.
32. Kabeya YMN, Ueno T, Yamamoto A, Kirisako T, Noda T, Kominami E, Ohsumi Y, Yoshimori T. LC3, a mammalian homologue of yeast Apg8p, is localized in autophagosome membranes after processing. EMBO J 2000; 19:5720–5728.
33. Choi S, Kim HJ. The Ca2+ channel TRPML3 specifically interacts with the mammalian ATG8 homologue GATE16 to regulate autophagy. Biochem Biophys Res Commun 2014;443:56–61.
34. Kondratskyi AYM, Kondratska K, Skryma R, Slomianny C, Prevarskaya N. Calcium-permeable ion channels in control of autophagy and cancer. Front Physiol 2013;4:272.
35. Ichai P, Samuel D. Management of Fulminant Hepatitis B. Curr Infect Dis Rep 2019;21:25.
36. Xiao F, Wang HW, Hu JJ, Tao R, Weng XX, Wang P, Wu D, Wang XJ, Yan WM, Xi D, Luo XP, Wan XY, Ning Q. Fibrinogen-like protein 2 deficiency inhibits virus-induced fulminant hepatitis through abrogating inflammatory macrophage activation. World J Gastroenterol 2022;28:479–496.
37. Diamond MS, Chen Y, Wu S, Guo G, Fei L, Guo S, Yang C, Fu X, Wu Y. Programmed death (PD)-1-deficient mice are extremely sensitive to murine hepatitis virus strain-3 (MHV-3) infection. PLoS Pathogens 2011;7:e1001347.
38. Zou Y, Chen T, Han M, Wang H, Yan W, Song G, Wu Z, Wang X, Zhu C, Luo X, Ning Q. Increased killing of liver NK cells by Fas/Fas ligand and NKG2D/NKG2D ligand contributes to hepatocyte necrosis in virus-induced liver failure. J Immunol 2010;184:466–475.
39. Yan M, Huo Y, Yin S, Hu H. Mechanisms of acetaminophen-induced liver injury and its implications for therapeutic interventions. Redox Biol 2018;17:274–283.
40. Kubes P, Mehal WZ. Sterile inflammation in the liver. Gastroenterology 2012;143:1158–1172.
41. Pope M, Cole E, Sinclair S, Parr R, Cruz B, Fingerote R, Chung S, Gorczynski R, Fung L. Pattern of disease after murine hepatitis virus strain 3 infection correlates with macrophage activation and not viral replication. J Virol 1995;69:5252–5260.
42. Saffarzadeh M, Juenemann C, Queisser MA, Lochnit G, Barreto G, Galuska SP, Lohmeyer J, Preissner KT. Neutrophil extracellular traps directly induce epithelial and endothelial cell death: a predominant role of histones. PLoS One 2012;7:e32366.
43. Sahoo M, Del Barrio L, Miller MA, Re F. Neutrophil elastase causes tissue damage that decreases host tolerance to lung infection with Burkholderia species. PLoS Pathog 2014;10:e1004327.
44. Mizushima N, Komatsu M. Autophagy: renovation of cells and tissues. Cell 2011;147:728–741.
45. Kim SW, Kim DH, Park KS, Kim MK, Park YM, Muallem S, So I, Kim HJ. Palmitoylation controls trafficking of the intracellular Ca2+ channel MCOLN3/TRPML3 to regulate autophagy. Autophagy 2018;15:327–340.
46. European Association for the Study of the Liver; Clinical Practice Guideline panel, Wendon J, Panel members, Cordoba J, Dhawan A, Larsen FS, Manns M, Samuel D, Simpson KJ, Yaron I, EASL Governing Board Representative, Bernardi M. EASL Clinical Practical Guidelines on the management of acute (fulminant) liver failure. J Hepatol 2017;66:1047–1081.
47. Sarin SK, Choudhury A, Sharma MK, Maiwall R, Al Mahtab M, Rahman S, Saigal S, Saraf N, Soin AS, Devarbhavi H, Kim DJ, Dhiman RK, Duseja A, Taneja S, Eapen CE, Goel A, Ning Q, Chen T, Ma K, Duan Z, Yu C, Treeprasertsuk S, Hamid SS, Butt AS, Jafri W, Shukla A, Saraswat V, Tan SS, Sood A, Midha V, Goyal O, Ghazinyan H, Arora A, Hu J, Sahu M, Rao PN, Lee GH, Lim SG, Lesmana LA, Lesmana CR, Shah S, Prasad VGM, Payawal DA, Abbas Z, Dokmeci AK, Sollano JD, Carpio G, Shresta A, Lau GK, Fazal Karim M, Shiha G, Gani R, Kalista KF, Yuen MF, Alam S, Khanna R, Sood V, Lal BB, Pamecha V, Jindal A, Rajan V, Arora V, Yokosuka O, Niriella MA, Li H, Qi X, Tanaka A, Mochida S, Chaudhuri DR, Gane E, Win KM, Chen WT, Rela M, Kapoor D, Rastogi A, Kale P, Rastogi A, Sharma CB, Bajpai M, Singh V, Premkumar M, Maharashi S, Olithselvan A, Philips CA, Srivastava A, Yachha SK, Wani ZA, Thapa BR, Saraya A, Shalimar Kumar A, Wadhawan M, Gupta S, Madan K, Sakhuja P, Vij V, Sharma BC, Garg H, Garg V, Kalal C, Anand L, Vyas T, Mathur RP, Kumar G, Jain P, Pasupuleti SSR, Chawla YK, Chowdhury A, Alam S, Song DS, Yang JM, Yoon EL; APASL ACLF Research Consortium (AARC) for APASL ACLF working Party. Acute-on-chronic liver failure: consensus recommendations of the Asian Pacific association for the study of the liver (APASL): an update. Hepatol Int 2019;13:353–390.
48. Yang W, Tao Y, Wu Y, Zhao X, Ye W, Zhao D, Fu L, Tian C, Yang J, He F, Tang L. Neutrophils promote the development of reparative macrophages mediated by ROS to orchestrate liver repair. Nat Commun 2019;10:1076.

49. Swamydas M, Luo Y, Dorf ME, Lionakis MS. Isolation of mouse neutrophils. Curr Protoc Immunol 2015;110:3–20, 1–3.20.15.
50. Brinkmann V, Laube B, Abu Abed U, Goosmann C, Zychlinsky A. Neutrophil extracellular traps: how to generate and visualize them. J Vis Exp 2010;36:1724.
51. Yang LLQ, Zhang X, Liu X, Zhou B, Chen J, Huang D, Li J, Li H, Chen F, Liu J, Xing Y, Chen X, Su S, Song E. DNA of neutrophil extracellular traps promotes cancer metastasis via CCDC25. Nature 2020; 583:133–138.

Received March 24, 2022. Accepted July 19, 2022.

Correspondence
Address correspondence to: Xiaojing Wang, MD, PhD, Department and Institute of Infectious Diseases, Tongji Hospital, Tongji Medical College, Huazhong University of Science and Technology, 1095 Jiefang Avenue, Wuhan 430030, Hubei, China. e-mail: wxjmoon@hotmail.com; fax: (86) 2783665959. Qin Ning, MD, PhD, Department and institute of infectious diseases, Tongji Hospital, Tongji Medical College, Huazhong University of Science and Technology, 1095 Jiefang Avenue, Wuhan 430030, Hubei, China. e-mail: qning@vip.sina.com; fax: (86) 2783665959.

Acknowledgments
The authors thank the members of the Institute of Infectious Diseases of Tongji Hospital for their pertinent advice, and also thank Dr Cailing Chen from the Department of Otolaryngology–Head and Neck Surgery of Tongji Hospital for her kindly suggestions.

CRediT Authorship Contributions
Xitang Li (Conceptualization: Equal; Data curation: Lead; Formal analysis: Lead; Software: Lead; Visualization: Lead; Writing – original draft: Lead)
Qiang Gao (Formal analysis: Equal; Investigation: Equal; Methodology: Equal; Project administration: Equal; Software: Lead)
Wenhui Wu (Formal analysis: Equal; Investigation: Equal; Methodology: Equal; Project administration: Equal; Software: Lead)
Suping Hai (Formal analysis: Equal; Investigation: Equal; Methodology: Equal; Project administration: Equal; Software: Lead)
Junjian Hu (Methodology: Supporting; Software: Supporting; Visualization: Supporting)
Jie You (Methodology: Supporting; Software: Supporting; Visualization: Supporting)
Da Huang (Formal analysis: Supporting; Methodology: Supporting; Software: Supporting)
Hongwu Wang (Methodology: Supporting; Resources: Supporting)
Di Wu (Resources: Supporting)
Meifang Han (Resources: Supporting)
Dong Xi (Resources: Supporting)
Weiming Yan (Methodology: Supporting)
Tao Chen (Methodology: Supporting)
Xiaoping Luo (Methodology: Supporting)
Qin Ning (Funding acquisition: Lead; Investigation: Equal; Methodology: Equal; Resources: Lead; Supervision: Lead)
Xiaojing Wang (Funding acquisition: Lead; Investigation: Lead; Methodology: Lead; Project administration: Lead; Resources: Lead; Supervision: Lead; Validation: Lead; Visualization: Lead)

Conflicts of interest
The authors disclose no conflicts.

Funding
Supported by the National Key Research and Development Program of China (2021YFC2600200), the National Natural Science Foundation of China (81974075), the National Youth Talent Support Program (0106540082), Wuhan Science and Technology Bureau (2020020601012236), Natural Science Foundation of Hubei Province (2020CFB767), and Youth Science Foundation of Tongji Hospital (2020YQ014).

Data availability
All data in our study are available upon request.